Available online at www.sciencedirect.com
ScienceDirect
Journal of Computational Physics 227 (2008) 3089–3113
JOURNAL OF COMPUTATIONAL PHYSICS
www.elsevier.com/locate/jcp

Augmented Riemann solvers for the shallow water equations over variable topography with steady states and inundation

David L. George *

Department of Mathematics, University of Utah, 155 South 1400 East, Room 233, Salt Lake City, UT 84112-0090, United States

Received 15 February 2007; received in revised form 26 October 2007; accepted 30 October 2007
Available online 22 November 2007

Abstract

We present a class of *augmented* approximate Riemann solvers for the shallow water equations in the presence of a variable bottom surface. These belong to the class of *simple* approximate solvers that use a set of propagating jump discontinuities, or *waves*, to approximate the true Riemann solution. Typically, a simple solver for a system of m conservation laws uses m such discontinuities. We present a four wave solver for use with the the shallow water equations—a system of two equations in one dimension. The solver is based on a decomposition of an augmented solution vector—the depth, momentum as well as momentum flux and bottom surface. By decomposing these four variables into four waves the solver is endowed with several desirable properties simultaneously. This solver is well-balanced: it maintains a large class of steady states by the use of a properly defined *steady state wave*—a stationary jump discontinuity in the Riemann solution that acts as a source term. The form of this wave is introduced and described in detail. The solver also maintains depth non-negativity and extends naturally to Riemann problems with an initial dry state. These are important properties for applications with steady states and inundation, such as tsunami and flood modeling. Implementing the solver with LeVeque's wave propagation algorithm [R.J. LeVeque, Wave propagation algorithms for multi-dimensional hyperbolic systems, J. Comput. Phys. 131 (1997) 327–335] is also described. Several numerical simulations are shown, including a test problem for tsunami modeling.

Keywords: Shallow water equations; Hyperbolic conservation laws; Finite volume methods; Godunov methods; Riemann solvers; Wave propagation; Shock capturing methods; Tsunami modeling

1. Introduction

The shallow water equations are a well known system of hyperbolic conservation laws, often with a source term, which in one dimension take the form

* Tel.: +1 206 356 2623; fax: +1 801 581 4148.
E-mail address: george@math.utah.edu
URL: http://www.math.utah.edu/~george

0021-9991/$ - see front matter © 2007 Elsevier Inc. All rights reserved.
doi:10.1016/j.jcp.2007.10.027

$$h_t + (hu)_x = 0, \tag{1a}$$

$$(hu)_t + \left(hu^2 + \frac{1}{2}gh^2\right)_x = -ghb_x, \tag{1b}$$

where g is the gravitational constant, $h(x,t)$ is the fluid depth, $u(x,t)$ is the vertically averaged horizontal fluid velocity, and $b(x)$ is the bottom surface elevation or *bathymetry*. Simple approximate Riemann solvers, described in Section 3, are used in the wave propagation methods that we use to solve hyperbolic systems. These methods belong to the class of finite volume Godunov-type methods and are described briefly in Section 2. We developed the augmented solver presented here while using shock capturing methods for tsunami modeling (*e.g.* [29,15,14,16]), due to the inadequacies of standard solvers for this application. Tsunami modeling demands certain properties of Riemann solvers, such as the preservation of delicate steady states and the maintenance of depth non-negativity in the Riemann solution, along with other standard properties sought in Riemann solvers such as suitable shock wave approximation and entropy requirements (for representing turbulent bores). See [4,27,36] for an overview of these latter topics. Additionally, inundation modeling requires Riemann solvers that generalize to problems with an initial dry state, as would occur right at the shoreline.

Non-trivial steady state solutions to (1) are physically prevalent in many shallow water applications and exist due to a balance of the flux divergence and the momentum source term due to variable bathymetry. This situation arises more generally for hyperbolic systems of the form

$$q_t + f(q)_x = \psi(q,x), \tag{2}$$

where $q \in \mathbb{R}^m$ is a vector of conserved quantities, $f(q) \in \mathbb{R}^m$ is the vector of corresponding fluxes, and $\psi(q,x) \in \mathbb{R}^m$ is a vector of source terms. Numerically preserving non-trivial steady states, or resolving small perturbations to them, when

$$f(q)_x \approx \psi(q,x) \tag{3}$$

yet both terms are relatively large, is a well known difficulty and one that has received considerable attention. See, for instance, [2,3,19,20,24,26]. For tsunami modeling this problem is particularly prevalent since the ocean at rest exhibits such a balance. Furthermore, in the deep ocean the depth h is several kilometers while a propagating tsunami typically has an amplitude of around a meter. With practical grid resolutions the traditional practice of fractional step integration of the source term can produce spurious waves of much greater magnitude than the actual tsunami.

An additional difficulty arises for many shallow water applications—the appearance and movement of dry regions with vanishing or zero depth. Preserving depth non-negativity while maintaining mass conservation is particularly difficult with most standard Riemann solvers. Again, this situation is exacerbated for tsunami modeling since numerical accuracy in the shallow inundation region is of the most interest, and this region also presents numerical difficulties such as shocks (representing turbulent bores) and drainage.

Developing well-balanced Riemann solvers specifically for the shallow water equations and the ocean at rest steady state in the presence of dry regions and variable bathymetry is an active topic of research. See, for instance, [2,11,12,5–7,31–33]. The solver presented in this paper appears to accomplish these goals for a larger class of problems in a more accurate and robust manner and has been applied to real flood and tsunami problems. The source code for the problems presented in this paper will be made available at the author's website. Adaptive two-dimensional software is also freely available and part of the GeoClaw software project [28].

2. The wave propagation algorithm

The methods described in this paper are implemented with the high resolution wave propagation algorithms developed by LeVeque [25,27], briefly described below. These methods are Godunov-type finite volume methods, *i.e.*, methods making use of Riemann problems to determine the numerical update at each time step. Godunov's original method [17] uses the Riemann solutions to determine cell interface fluxes at each time step. Rather than using interface fluxes directly, in LeVeque's wave propagation algorithm the waves arising in Riemann solutions are directly re-averaged onto adjacent grid cells in order to update the numerical solution. LeVeque's method is therefore applicable to hyperbolic systems of the form

$$q_t + A(q,x)q_x = 0, \tag{4}$$

where $q \in \mathbb{R}^m$ and $A(q,x) \in \mathbb{R}^{m\times m}$, which include conservation laws

$$q_t + f(q)_x = 0, \tag{5}$$

where $A(q,x) = A(q) = f'(q)$, as well as non-conservative systems where there is no flux function. The first order one-dimensional wave propagation method has the form

$$Q_i^{n+1} = Q_i^n - \frac{\Delta t}{\Delta x}(\mathcal{A}^+\Delta Q_{i-1/2}^n + \mathcal{A}^-\Delta Q_{i+1/2}^n), \tag{6}$$

where Q_i^n is a numerical approximation to $\frac{1}{\Delta x}\int_{\mathcal{C}_i} q(x,t^n)\mathrm{d}x$, with $\mathcal{C}_i = [x_{i-1/2}, x_{i+1/2}]$, $\Delta x = (x_{i+1/2} - x_{i-1/2})$ and $\Delta t = (t^{n+1} - t^n)$. The *fluctuations* $\mathcal{A}^\pm\Delta Q_{i\pm1/2}^n$ are determined by solutions to Riemann problems at the cell interfaces at $x_{i\pm1/2}$. The term $\mathcal{A}^+\Delta Q_{i-1/2}^n$ represents the net updating contribution from the rightward moving waves into grid cell $\mathcal{C}_i$ from the left interface, and $\mathcal{A}^-\Delta Q_{i+1/2}^n$ represents the net updating contribution from the leftward moving waves into cell $\mathcal{C}_i$ from the right interface. Calculating $\mathcal{A}^\pm\Delta Q_{i\pm1/2}^n$ from the waves in the Riemann solutions is straightforward and described briefly in the next section.

The wave propagation method (6) can be extended to formal second order accuracy by including correction terms:

$$Q_i^{n+1} = Q_i^n - \frac{\Delta t}{\Delta x}(\mathcal{A}^+\Delta Q_{i-1/2}^n + \mathcal{A}^-\Delta Q_{i+1/2}^n) - \frac{\Delta t}{\Delta x}(\widetilde{F}_{i+1/2}^n - \widetilde{F}_{i-1/2}^n). \tag{7}$$

Like the fluctuations $\mathcal{A}^\pm\Delta Q_{i\pm1/2}^n$, the second order correction terms $\widetilde{F}_{i\pm1/2}^n$ can be determined entirely by the waves in the Riemann problems at $x_{i\pm1/2}$. The determination of the second order corrections will be discussed in more detail in Section 3.1. In order to prevent spurious numerical oscillations near discontinuities or steep gradients, the correction term $\widetilde{F}_{i-1/2}^n$ is limited by the use of a limiter function that assesses local variation in the solution. There are many standard limiter functions that ensure TVD stability of the solution (see [35] or [27] for a discussion).

Extension to multiple dimensions is possible by solving one-dimensional normal Riemann problems, and again including second order correction terms—which include approximations to cross derivatives in multiple dimensions. As in one dimension, all of these second order terms can be determined by the waves in Riemann solutions. In two dimensions, hyperbolic systems of the form

$$q_t + A(q,x,y)q_x + B(q,x,y)q_y = 0, \tag{8}$$

where $q \in \mathbb{R}^m$, $A(q,x,y), B(q,x,y) \in \mathbb{R}^{m\times m}$, are approximated by a wave propagation algorithm of the form

$$\begin{aligned} Q_{ij}^{n+1} = Q_{ij}^n &- \frac{\Delta t}{\Delta x}(\mathcal{A}^+\Delta Q_{i-1/2,j}^n + \mathcal{A}^-\Delta Q_{i+1/2,j}^n) - \frac{\Delta t}{\Delta y}(\mathcal{B}^+\Delta Q_{i,j-1/2}^n + \mathcal{B}^-\Delta Q_{i,j+1/2}^n) \\ &- \frac{\Delta t}{\Delta x}(\widetilde{F}_{i+1/2,j}^n - \widetilde{F}_{i-1/2,j}^n) - \frac{\Delta t}{\Delta y}(\widetilde{G}_{i,j+1/2}^n - \widetilde{G}_{i,j-1/2}^n). \end{aligned} \tag{9}$$

The terms $\mathcal{A}^\pm\Delta Q_{i\pm1/2,j}^n$ and $\widetilde{F}_{i\pm1/2,j}^n$ are determined by Riemann problems in the x-direction at the left and right edges of the rectangular cell $\mathcal{C}_{ij}$, and similarly $\mathcal{B}^\pm\Delta Q_{i,j\pm1/2}^n$ and $\widetilde{G}_{i,j\pm1/2}^n$ are determined by Riemann problems in the y-direction at the top and bottom of $\mathcal{C}_{ij}$. Again, the second order correction terms $\widetilde{F}_{i\pm1/2,j}^n$ and $\widetilde{G}_{i,j\pm1/2}^n$ are limited near shocks or gradients to prevent oscillations due to numerical dispersion. Because one-dimensional Riemann solvers are used for the method (9), in this paper we will concentrate on the one-dimensional problem and algorithms. For more detail on the extension of the wave propagation algorithm to multiple dimensions using one-dimensional Riemann solvers, see [27]. For additional detail on using the Riemann solver presented in this paper in two dimensions see [14].

3. Standard Riemann solvers for wave propagation

The wave propagation algorithms introduced in the previous section require a Riemann solver to determine the updating fluctuations $\mathcal{A}^\pm\Delta Q_{i-1/2}^n$ and second-order correction term $\widetilde{F}_{i-1/2}^n$ at a grid cell interface $x_{i-1/2}$. The Riemann solver is the primary topic of this paper. For more details on the wave propagation algorithm itself,

we refer the reader to standard references such as [25,27]. Recall that a Riemann solver provides an exact or approximate weak solution to the hyperbolic PDE given initial data that is piecewise constant with a single jump discontinuity. We will look at the Riemann problem for the system (4) with initial data

$$q(x,t^n) = \begin{cases} Q_{i-1}^n & \text{if } x < x_{i-1/2}, \\ Q_i^n & \text{if } x > x_{i-1/2}. \end{cases} \tag{10}$$

One type of approximate solver for (10), which we call a *simple solver* (following [4]), approximates the true Riemann solution as a piecewise constant solution with M_w propagating jump discontinuities, or *waves*, $\mathcal{W}_{i-1/2}^p \in \mathbb{R}^m$, for $p = 1, \ldots, M_w$. Each wave $\mathcal{W}_{i-1/2}^p$ propagates with a constant wave-speed $s_{i-1/2}^p$. Note that the initial data must satisfy

$$Q_i^n - Q_{i-1}^n = \sum_{p=1}^{M_w} \mathcal{W}_{i-1/2}^p. \tag{11}$$

Eq. (11) suggests a means for determining the approximate Riemann solution—simply use a decomposition of the initial data into a set of vectors $r_{i-1/2}^p \in \mathbb{R}^m$, for $p = 1, \ldots, M_w$:

$$Q_i - Q_{i-1} = \sum_{p=1}^{M_w} \mathcal{W}_{i-1/2}^p = \sum_{p=1}^{M_w} \alpha_{i-1/2}^p r_{i-1/2}^p, \tag{12a}$$

where $\mathcal{W}_{i-1/2}^p = \alpha_{i-1/2}^p r_{i-1/2}^p$. (To ease notation we will now suppress the time superscript, n, it being understood that all quantities are determined explicitly at time t^n.) Given the waves $\mathcal{W}_{i-1/2}^p$ and wave-speeds $s_{i-1/2}^p$, the fluctuations are defined by

$$\mathcal{A}^- \Delta Q_{i-1/2} = \sum_{\{p: s_{i-1/2}^p < 0\}} s_{i-1/2}^p \mathcal{W}_{i-1/2}^p, \tag{12b}$$

$$\mathcal{A}^+ \Delta Q_{i-1/2} = \sum_{\{p: s_{i-1/2}^p > 0\}} s_{i-1/2}^p \mathcal{W}_{i-1/2}^p. \tag{12c}$$

The vector $r_{i-1/2}^p$ and associated wave-speed $s_{i-1/2}^p$ are preselected based on the characteristic structure of the PDE, and are typically functions of the initial Riemann data. Typically one chooses $M_w = m$, and linearly independent vectors $r_{i-1/2}^p$, for $p = 1, \ldots, m$, so that the coefficients $\alpha_{i-1/2}^p \in \mathbb{R}$ in (12a) are uniquely determined. However, this is not strictly necessary. In fact, with some approximate solvers providing more than m waves in the case of a transonic rarefaction is necessary to prevent convergence to entropy violating *expansion shocks*—non-physical weak solutions. See [27] for details of this problem with some common Riemann solvers and some appropriate entropy fixes. A common choice for the pair $\{r_{i-1/2}^p, s_{i-1/2}^p\}$ is the pth eigenpair of a local linear approximation to $A(q,x)$ at $x_{i-1/2}$, since then the approximate Riemann solution corresponds to the true solution of the linearized problem.

A widely used linearization for a conservation law of the form (5) is the Roe solver [34], where $\{r_{i-1/2}^p, s_{i-1/2}^p\}$ is chosen to be the pth eigenpair $\{\hat{r}_{i-1/2}^p, \hat{\lambda}_{i-1/2}^p\}$ of the Roe Jacobian matrix $\widehat{A}_{i-1/2} = A(\widehat{Q}_{i-1/2})$, where $\widehat{Q}_{i-1/2}$ is the Roe average of Q_i and Q_{i-1}. (We will use a hat to denote Roe averaged quantities throughout this paper.) Given two states, Q_i and Q_{i-1}, by definition the Roe averaged Jacobian satisfies the following property:

$$\widehat{A}_{i-1/2}(Q_i - Q_{i-1}) = f(Q_i) - f(Q_{i-1}). \tag{13}$$

With the Roe solver if the true Riemann solution corresponds to a single shock-wave, *i.e.* the initial Riemann data lies on a single Hugoniot-locus (see *e.g.* [27]), then the Roe solver produces the exact solution. This follows from (13) and the Rankine–Hugoniot conditions for a shock wave moving with speed s:

$$f(Q_i) - f(Q_{i-1}) = s(Q_i - Q_{i-1}), \tag{14}$$

which together imply that $Q_i - Q_{i-1}$ is an eigenvector of $\widehat{A}_{i-1/2}$ with eigenvalue s. The decomposition (12a) thus provides the exact solution.

A consistent alternative approach to (12) for a conservation law, is to perform a decomposition of the flux

$$f(Q_i) - f(Q_{i-1}) = \sum_{p=1}^{M_w} \mathcal{Z}^p_{i-1/2} = \sum_{p=1}^{M_w} \beta^p_{i-1/2} r^p_{i-1/2}. \tag{15a}$$

The waves $\mathcal{Z}^p_{i-1/2} = \beta^p_{i-1/2} r^p_{i-1/2}$, for $p = 1, \ldots, M_w$, now represent propagating jumps in the flux, and the fluctuations are therefore defined by

$$\mathcal{A}^- \Delta Q_{i-1/2} = \sum_{\{p: s^p_{i-1/2} < 0\}} \mathcal{Z}^p_{i-1/2}, \tag{15b}$$

$$\mathcal{A}^+ \Delta Q_{i-1/2} = \sum_{\{p: s^p_{i-1/2} > 0\}} \mathcal{Z}^p_{i-1/2}. \tag{15c}$$

This has been referred to as the *f*-wave method [3], since the waves carry units of flux. Typically the pairs $\{r^p_{i-1/2}, s^p_{i-1/2}\}$ are the same that would be used in (12). (In the event that $s^p_{i-1/2} = 0$ and $||\mathcal{Z}^p_{i-1/2}|| > 0$ for some p, it is necessary for numerical conservation to include the stationary wave $\mathcal{Z}^p_{i-1/2}$ into the fluctuations, such as including half of it in each of (15b) and (15c). However, for many choices of $\{r^p_{i-1/2}, s^p_{i-1/2}\}$, $s^p_{i-1/2} = 0$ implies that $||Z^p_{i-1/2}|| = 0$. See [3].) The consistency of (15) is not surprising if one considers a linear problem with $f(q) = Aq$, where the true Riemann solution has jump discontinuities proportional to the eigenvectors of the Jacobian A propagating at the speeds of the eigenvalues, and the jumps in the flux are therefore proportional to the jumps in the solution but multiplied by the corresponding eigenvalues. Moreover, for the nonlinear problem the Rankine–Hugoniot jump condition (14) implies that across a discontinuity the jump in flux is equal to the jump in the solution multiplied by the speed of the propagating discontinuity.

If Roe eigenpairs are used, the decompositions in (12) and (15) produce identical fluctuations since (12a), (13) and (15a) imply that $\beta^p_{i-1/2} = s^p_{i-1/2} \alpha^p_{i-1/2}$ for $p = 1, \ldots, m$.

3.1. Second-order correction terms

The second order correction term $\widetilde{F}^n_{i-1/2}$ improves the order of accuracy of the wave propagation algorithm, at least where the solution is smooth. It can be determined entirely by the waves in the Riemann problem at $x_{i-1/2}$. If a solver of the form (12) is used, the correction term is given by

$$\widetilde{F}_{i-1/2} = \frac{1}{2} \sum_{p=1}^{M_w} |s^p_{i-1/2}| \left(1 - \frac{\Delta t}{\Delta x} |s^p_{i-1/2}|\right) \widetilde{\mathcal{W}}^p_{i-1/2}, \tag{16}$$

where $\widetilde{\mathcal{W}}^p_{i-1/2}$ is a limited version of the wave $\mathcal{W}^p_{i-1/2}$ using a TVD limiter. If a solver of the form (15) is used, the correction term is given by

$$\widetilde{F}_{i-1/2} = \frac{1}{2} \sum_{p=1}^{M_w} \operatorname{sgn}(s^p_{i-1/2}) \left(1 - \frac{\Delta t}{\Delta x} |s^p_{i-1/2}|\right) \widetilde{\mathcal{Z}}^p_{i-1/2}, \tag{17}$$

where $\widetilde{\mathcal{Z}}^p_{i-1/2}$ is a limited version of the wave $\mathcal{Z}^p_{i-1/2}$, again using a TVD limiter. See [27] for details.

3.2. Properties and inadequacies of standard solvers

The difference between a standard solver based on a decomposition of the solution (12) and one based on a flux decomposition (15) may seem mostly aesthetic since both provide consistent definitions for the fluctuations $\mathcal{A}^\pm \Delta Q_{i-1/2}$ by approximating the true nonlinear Riemann solution. However, there are various motivations and drawbacks to each. First, one caveat to using (12) for a conservation law, in which $A(q)$ in (4) corresponds to the flux Jacobian $f'(q)$, is that numerical conservation is guaranteed only if the fluctuations satisfy

$$f(Q_i) - f(Q_{i-1}) = \mathcal{A}^+ \Delta Q_{i-1/2} + \mathcal{A}^- \Delta Q_{i-1/2}. \tag{18}$$

The requirement (18) is satisfied if (12) is based on a Roe solver. However, using Roe eigenpairs has some drawbacks such as failing to preserve depth non-negativity in the case of the shallow water equations, and

requiring entropy fixes to prevent non-physical solutions (see [34,27] or [14]). A more general choice of pairs $\{r^p_{i-1/2}, s^p_{i-1/2}\}$ for (12) will not guarantee a conservative numerical update. On the other hand, an *f*-wave approach defined by (15) always produces a conservative numerical method since (18) is automatically satisfied, as long as $s^p_{i-1/2} \neq 0$ for $p = 1, \ldots, M_w$. (An easy fix is available if $s^p_{i-1/2} = 0$ and $||\mathcal{Z}^p_{i-1/2}|| > 0$ for some p, as mentioned in the last section.)

Unfortunately, for shallow water applications there is an inherent weakness to the *f*-wave approach; since the depth is not included in the decomposition there is no clear way to prevent depth non-negativity in the Riemann solution—an important property for shallow water applications with inundation. We will refer to solvers that maintain depth non-negativity in the approximate solution as *depth positive semidefinite*. Approximate Riemann solvers are generally not depth positive semidefinite. Exceptions include some of the HLL-type solvers [21], such as the HLLE solver [9,10]. These solvers are not based on a characteristic eigendecomposition such as (12a) or (15a) with eigenvectors $r^p_{i-1/2}$. The HLL-type solvers are not well-balanced, and require a rather involved modification in order to properly preserve steady states for the shallow water equations; see [13,29] for such a procedure. However, the solver described in the final sections of this paper incorporates the depth positive semidefinite feature of the HLLE solver, while based on a simple eigendecomposition framework.

Another weakness of simple approximate solvers with m discontinuities is that they inaccurately represent a true Riemann solution if it has large rarefaction waves. The most important such case is a Riemann solution with a transonic rarefaction that spreads in both directions. It is well known that approximating such a wave with a single discontinuity can produce non-physical entropy violating numerical solutions. One possible fix to this problem is to provide two discontinuities, one moving in each direction, to approximate the single transonic rarefaction. Of course, then a decomposition of the form (12a) or (15a) is not uniquely determined, and some scheme must be devised to determine the coefficients $\alpha^p_{i-1/2}$ or $\beta^p_{i-1/2}$, for $p = 1, \ldots, (m+1)$, in those under-determined systems. See [27] for some examples of such schemes.

3.3. Solvers with more than m waves

Another possibility for providing more than m waves is to use a decomposition of an augmented vector with M_w components ($M_w > m$) into M_w linearly independent vectors $r^p_{i-1/2} \in \mathbb{R}^{M_w}$, providing unique coefficients. For instance, in [30] LeVeque and Pelanti explore decompositions of the form

$$\begin{bmatrix} Q_i - Q_{i-1} \\ f(Q_i) - f(Q_{i-1}) \end{bmatrix} = \sum_{p=1}^{2m} \alpha^p_{i-1/2} \begin{bmatrix} r^p_{i-1/2} \\ z^p_{i-1/2} \end{bmatrix}, \tag{19}$$

where $r^p_{i-1/2} \in \mathbb{R}^m$, $z^p_{i-1/2} \in \mathbb{R}^m$ and again each wave propagates at an associated speed $s^p_{i-1/2}$, for $p = 1, \ldots, 2m$. Although this decomposition contains $2m$ waves with $2m$ components, only m components of those $2m$ waves are needed to define the fluctuations. Since both the solution and the flux are decomposed in (19), the fluctuations could be defined similarly to the fluctuations in (12) with $\alpha^p_{i-1/2} r^p_{i-1/2} = \mathcal{W}^p_{i-1/2}$, or similarly to the fluctuations in (15) with $\alpha^p_{i-1/2} z^p_{i-1/2} = \mathcal{Z}^p_{i-1/2}$. If one defines the vectors $z^p_{i-1/2}$ by $z^p_{i-1/2} = s^p_{i-1/2} r^p_{i-1/2}$, these two alternatives yield identical conservative fluctuations. It should be noted that the vector $(Q_i - Q_{i-1}, f(Q_i) - f(Q_{i-1}))^T \in \mathbb{R}^{2m}$ actually lies in the m-dimensional subspace spanned by $(\hat{r}^n_{i-1/2}, \hat{\lambda}^p_{i-1/2}\hat{r}^p_{i-1/2})^T \in \mathbb{R}^{2m}$, where $\{\hat{r}^p_{i-1/2}, \hat{\lambda}^p_{i-1/2}\}$, $p = 1, \ldots, m$, are the m eigenpairs of a Roe averaged Jacobian $\hat{A}_{i-1/2}$. This follows from (13). Therefore the standard method (12), the *f*-wave method (15) and the augmented decomposition (19) are all equivalent when Roe eigenpairs are used. For a more complete discussion of (19) using other vectors, and its relation to relaxation to relaxation solvers, see [30].

4. Augmented Riemann solvers for the shallow water equations

In this section we introduce a novel approximate solver for the shallow water equations, for both the homogeneous case and more generally in the presence of a source term. The motivation for this solver is that it simultaneously possesses desirable qualities of the Roe solver [34], HLLE-type solvers [9,10] and the *f*-wave approach [3] without the inherit weaknesses of each. For instance, like the HLLE solver, it is depth positive

semidefinite—an important property for accurate inundation modeling. Additionally, like the Roe solver, it provides the exact solution in the event of a single-shock Riemann problem—a desirable property for shock-capturing schemes. Further, by providing more than two waves, the solver has a natural entropy fix and provides a better approximation for problems with large rarefactions. The solver is well-balanced in that it preserves a large class of steady states, even non-stationary steady states with non-zero fluid velocity. We will show how this well-balanced inclusion of the source term is accomplished in a simple solver framework, where the Riemann solver is entirely defined by a set of linearly independent vectors and associated wave speeds, so that a simple decomposition of initial Riemann data uniquely determines the approximate solution.

4.1. An augmented solver for the homogeneous shallow water equations

We first describe the approximate Riemann solver for the homogeneous shallow water equations

$$h_t + (hu)_x = 0, \tag{20a}$$

$$(hu)_t + \left(hu^2 + \frac{1}{2}gh^2\right)_x = 0. \tag{20b}$$

In Section 4.2 we describe the full solver for the non-homogeneous system, which reduces to the solver described in this section when there is no source term. For the homogeneous system, the solver is related to (19), in that we use a decomposition of the flux and solution into a set of vectors. However, note that the decomposition (19) for the shallow water equations would decompose two identical components since both the second component of the solution q and the first component of the flux $f(q)$ are equal the momentum hu. Instead we consider a decomposition of the form

$$\begin{bmatrix} H_i - H_{i-1} \\ HU_i - HU_{i-1} \\ \varphi(Q_i) - \varphi(Q_{i-1}) \end{bmatrix} = \sum_{p=1}^{3} \alpha_{i-1/2}^p w_{i-1/2}^p, \tag{21}$$

where $Q_i = (H_i, HU_i)^T$ is the numerical solution for $q = (h, hu)^T$ in $\mathcal{C}_i$, $\varphi(q) = (hu^2 + \frac{1}{2}gh^2)$ is the momentum flux, and $w_{i-1/2}^p \in \mathbb{R}^3$, for $p = 1, \ldots, 3$, is a chosen set of independent vectors. Note that the first two of the three components in (21) represent a decomposition of the solution $Q_i - Q_{i-1} \in \mathbb{R}^2$, and the last two of the three components represent a decomposition of the flux $f(Q_i) - f(Q_{i-1}) \in \mathbb{R}^2$. In order to ensure conservation, regardless of the form of $w_{i-1/2}^p$, we use the last two of three components of the decomposition (21) to define the updating fluctuations. That is, we define flux waves $\mathcal{Z}_{i-1/2}^p \in \mathbb{R}^2$, for $p = 1, \ldots, 3$, by

$$\mathcal{Z}_{i-1/2}^p = [\mathbf{0}_{2\times 1} \quad \mathbf{I}_{2\times 2}]\alpha_{i-1/2}^p w_{i-1/2}^p, \tag{22}$$

where $\mathbf{I}_{2\times 2}$ is the two by two identity, and $\mathbf{0}_{2\times 1}$ the two by one zeros matrix. (The matrix multiplication in (22) simply selects the last two components of $\alpha_{i-1/2}^p w_{i-1/2}^p \in \mathbb{R}^3$, for each $p = 1, \ldots, 3$.) We then define the fluctuations by

$$\mathcal{A}^- \Delta Q_{i-1/2} = \sum_{\{p: s_{i-1/2}^p < 0\}} \mathcal{Z}_{i-1/2}^p, \tag{23a}$$

$$\mathcal{A}^+ \Delta Q_{i-1/2} = \sum_{\{p: s_{i-1/2}^p > 0\}} \mathcal{Z}_{i-1/2}^p, \tag{23b}$$

exactly as in (15). This implies that the updating fluctuations are ultimately determined by a flux decomposition similar to the f-wave approach (15). However, we have decomposed the flux uniquely into three waves rather than two. As described in Section 5, this allows a more accurate approximation to Riemann problems with a large rarefaction and a natural entropy fix for transonic rarefactions. Moreover, as will be shown, including $H_i - H_{i-1}$ in the decomposition makes it possible to create updating fluctuations that correspond to using a depth positive semidefinite Riemann solver, even though our fluctuations are based on flux waves. Additionally, when we include source terms, it will be shown that including both the depth and fluxes in our decomposition will be necessary to precisely preserve steady states.

Of course, we must choose vectors $w^p_{i-1/2} \in \mathbb{R}^3$ and associated wave speeds $s^p_{i-1/2}$, for $p = 1, \ldots, 3$. The first and third pairs $\{w^{1,3}_{i-1/2}, s^{1,3}_{i-1/2}\}$ will be related to the original two fields of the shallow water equations. (We use $p = 1$ and $p = 3$ for these pairs since, as we will see, $s^1_{i-1/2} < s^2_{i-1/2} < s^3_{i-1/2}$.) The Jacobian of the shallow water system (20) has eigenpairs $\{r(q), \lambda(q)\}$ given by

$$\{r^{\pm}(q), \lambda^{\pm}(q)\} = \{(1, u \pm \sqrt{gh})^T, u \pm \sqrt{gh}\}. \tag{24}$$

We choose

$$\{w^1_{i-1/2}, s^1_{i-1/2}\} = \left\{(1, \check{s}^-_{i-1/2}, (\check{s}^-_{i-1/2})^2)^T, \check{s}^-_{i-1/2}\right\}, \tag{25a}$$

$$\{w^3_{i-1/2}, s^3_{i-1/2}\} = \left\{(1, \check{s}^+_{i-1/2}, (\check{s}^+_{i-1/2})^2)^T, \check{s}^+_{i-1/2}\right\}, \tag{25b}$$

where $\check{s}^-_{i-1/2}$ and $\check{s}^+_{i-1/2}$ are defined by

$$\check{s}^-_{i-1/2} = \min(\lambda^-(Q^n_{i-1}), \hat{\lambda}^-_{i-1/2}), \tag{26a}$$

$$\check{s}^+_{i-1/2} = \max(\lambda^+(Q^n_i), \hat{\lambda}^+_{i-1/2}), \tag{26b}$$

where $\hat{\lambda}^{\pm}_{i-1/2}$ are the eigenvalues of the Roe averaged Jacobian $\widehat{A}_{i-1/2}$. (For the definition and derivation of the Roe averages for the shallow water equations see [34] or [27].) We will refer to the speeds (26) as the *Einfeldt speeds*, since they were suggested by Einfeldt for use with the HLLE solver ([21,9,10]) in order to preserve depth non-negativity. (We use a *check* $\check{}$ in the notation of quantities related to the HLLE solver, and a hat for Roe averages.)

The additional pair $\{w^2_{i-1/2}, s^2_{i-1/2}\}$ needed for (21) can be chosen in various ways. We will refer to the resulting second wave $\mathcal{Z}^2_{i-1/2}$ as the *corrector wave*, since it corrects for inaccurate, non-conservative or entropy violating approximate Riemann solutions with only two waves. For now we will let

$$\{w^2_{i-1/2}, s^2_{i-1/2}\} = \left\{(0,\ 0,\ 1)^T, \frac{1}{2}(\check{s}^-_{i-1/2} + \check{s}^+_{i-1/2})\right\}. \tag{27}$$

In Section 5 we will describe how some simple assessments of the exact Riemann structure can optionally be used to better choose $\{w^2_{i-1/2}, s^2_{i-1/2}\}$ and improve the accuracy of the approximate solution. By choosing (27), the Riemann solver corresponds to the Roe solver for shock problems lacking a rarefaction, in which the Einfeldt speeds (26) correspond to the Roe eigenvalues. This is because the vector $(Q_i - Q_{i-1}, \varphi(Q_i) - \varphi(Q_{i-1}))^T \in \mathbb{R}^3$ lies in the 2-dimensional subspace spanned by the vectors $w^1_{i-1/2}$ and $w^3_{i-1/2}$ in (25) (following from (13)). Therefore, $\alpha^2_{i-1/2} = 0$, there is no second wave, and the solution and flux are decomposed into Roe eigenvectors. More generally, for Riemann problems without a significant or *strong* rarefaction, the Einfeldt speeds correspond to, or are at least close to the Roe eigenvalues. (This follows from conservation of the Roe solver—see [14].) It therefore follows that the second wave $\mathcal{Z}^2_{i-1/2}$ will be small in magnitude for such problems, even when one of the Einfeldt speeds is not exactly the corresponding Roe eigenvalue. An optional correction for problems with a large rarefaction will be described in Section 5.

When using (27), in order to guarantee conservation for Riemann problems in which $s^2_{i-1/2} = 0$, the wave $\mathcal{Z}^2_{i-1/2}$ should be divided into $\mathcal{A}^+\Delta Q_{i-1/2}$ and $\mathcal{A}^-\Delta Q_{i-1/2}$. This is because, unlike with $p = 1$ and $p = 3$, with $p = 2$, $s^2_{i-1/2} = 0$ does not imply that $\mathcal{Z}^2_{i-1/2} = 0$. This is not unique to this Riemann solver, but is required of any approximate Riemann solver based on a flux decomposition, where the flux is decomposed into a stationary vector (see [3]). In exact Riemann solutions to conservation laws the Rankine–Hugoniot condition implies that a jump in the flux should not occur across a stationary discontinuity, and further for the homogeneous shallow water equations a discontinuity in $(h, hu, \varphi)^T$ is always proportional to $(1, s, s^2)^T$, where s is the speed of the discontinuity. In the next section we show how a jump in the flux across a stationary discontinuity acts as a concentrated source term.

The choice (27) implies that the mass (depth) update defined by (21)–(23) is equivalent to the HLLE solver. This is detailed in [14], but can be seen by considering the following argument. The HLLE solver uses the speeds (26) to define two propagating discontinuities, and then a middle state between the two discontinuities is determined such that numerical conservation is maintained. The first component of the HLLE middle state, here denoted $\check{H}^*_{i-1/2}$, is given by

$$\check{H}^*_{i-1/2} = \frac{HU_{i-1} - HU_i + \check{s}^+_{i-1/2} H_i - \check{s}^-_{i-1/2} H_{i-1}}{\check{s}^+_{i-1/2} - \check{s}^-_{i-1/2}}. \tag{28}$$

Note that if (27) is used, the first component of $\mathcal{Z}^2_{i-1/2}$ must be zero. Therefore, the mass is updated by only two discontinuities, the first components of $\mathcal{Z}^1_{i-1/2}$ and $\mathcal{Z}^3_{i-1/2}$, both propagating at the same speeds (26) used by the HLLE solver. Since the HLLE solver is depth positive semidefinite, $\check{H}^*_{i-1/2} \geqslant 0$, the updating fluctuations (23) when using (27) correspond to a depth positive semidefinite Riemann solver.

One advantage to the solver presented here over the standard HLLE solver is that we will be able to include the contribution of a source term with the introduction of another wave while maintaining steady states precisely, as well as maintaining the depth positive semidefinite feature. This is described in the following sections where we generalize the solver to include problems with a source term.

4.2. Including the source term

Over variable bathymetry the shallow water equations (1) possess a source term that contributes to momentum. Numerical treatment of this source term is important for applications such as tsunami modeling since the source term and flux divergence must balance properly in the numerical method in order to accurately model the small perturbations that represent the tsunami. This is not necessarily an issue of order of accuracy of the numerical method—a high-order method can fail at preserving this balance on practical grid resolutions. It is necessary to preserve the ocean at rest steady state even on very coarse grid resolutions. This is especially true since we use our wave-propagation method together with adaptive mesh refinement, which puts regions at steady state on extremely coarse grid resolutions for efficiency (see [15,16]).

The standard approach of fractional stepping to include the source term fails at preserving the required balance, as is well known (*e.g.* [3,4,14,26]). Instead, we include the effect of the source term by introducing a fourth wave to our solver, and including the bottom elevation $b(x)$ into our decomposition. That is, we generalize (21) to include decompositions of the form

$$\begin{bmatrix} H_i - H_{i-1} \\ HU_i - HU_{i-1} \\ \varphi(Q_i) - \varphi(Q_{i-1}) \\ B_i - B_{i-1} \end{bmatrix} = \sum_{p=0}^{3} \alpha^p_{i-1/2} w^p_{i-1/2}, \tag{29}$$

where B_i and B_{i-1} are cell-averaged approximations to the bottom elevation in $\mathcal{C}_i$ and $\mathcal{C}_{i-1}$. Now we must choose $w^p_{i-1/2} \in \mathbb{R}^4$, and associated wave speeds $s^p_{i-1/2}$ for $p = 0, \ldots, 3$. (We index the new wave with $p = 0$ to indicate that, as we will see, this wave is stationary, $s^0_{i-1/2} = 0$.) As with the three-wave solver for the homogeneous case, we use the second and third components of $\alpha^p_{i-1/2} w^p_{i-1/2} \in \mathbb{R}^4$ to define $\mathcal{Z}^p_{i-1/2} \in \mathbb{R}^2$. That is, for each p, we let

$$\mathcal{Z}^p_{i-1/2} = [\,\mathbf{0}_{2\times 1} \quad \mathbf{I}_{2\times 2} \quad \mathbf{0}_{2\times 1}\,]\alpha^p_{i-1/2} w^p_{i-1/2} \tag{30}$$

and again define the fluctuations by (23), noting that now there are four waves $\mathcal{Z}^p_{i-1/2}$, $p = 0, \ldots, 3$, and the wave corresponding to $p = 0$ is not included in the fluctuations since $s^0_{i-1/2} = 0$. The effect of the source term is actually included in this construction of the fluctuations by a proper choice of $w^0_{i-1/2}$, as described below and in Section 4.2.1.

One interpretation of the decomposition (29) is that it is a simple wave based solver of the form (12) for a nonlinear homogeneous hyperbolic system of the form (4), with $m = 4$. The shallow water Eqs. (1) are equivalent to such a system, which we will write as

$$\tilde{q}_t + W(\tilde{q})\tilde{q}_x = 0, \tag{31}$$

where

$$\tilde{q} = (h,\ hu,\ \varphi,\ b)^T \tag{32}$$

is an augmented state variable and

$$W(\tilde{q}) = \begin{bmatrix} 0 & 1 & 0 & 0 \\ -u^2 + gh & 2u & 0 & gh \\ 0 & -u^2 + gh & 2u & 2ugh \\ 0 & 0 & 0 & 0 \end{bmatrix}. \tag{33}$$

The eigenpairs of the matrix (33) are

$$\{r^0(\tilde{q}), \lambda^0(\tilde{q})\} = \left\{ \left(\frac{gh}{\lambda^1(\tilde{q})\lambda^3(\tilde{q})}, 0, -gh, 1 \right)^T, 0 \right\}, \tag{34a}$$

$$\{r^1(\tilde{q}), \lambda^1(\tilde{q})\} = \left\{ (1, \lambda^1(\tilde{q}), (\lambda^1(\tilde{q}))^2, 0)^T, u - \sqrt{gh} \right\}, \tag{34b}$$

$$\{r^2(\tilde{q}), \lambda^2(\tilde{q})\} = \{(0, 0, 1, 0)^T, 2u\}, \tag{34c}$$

$$\{r^3(\tilde{q}), \lambda^3(\tilde{q})\} = \left\{ (1, \lambda^3(\tilde{q}), (\lambda^3(\tilde{q}))^2, 0)^T, u + \sqrt{gh} \right\}. \tag{34d}$$

Note that the form of $r^p((\tilde{q}))$ resembles the vectors $w^p_{i-1/2}$, for $p = 1, \ldots, 3$, used in the homogeneous solver (21) with an additional fourth component equal to zero. Therefore, we continue to use these three vectors, adding a fourth component equal to zero, and keep the same wave speeds, which gives pairs

$$\{w^1_{i-1/2}, s^1_{i-1/2}\} = \{(1, \check{s}^-_{i-1/2}, (\check{s}^-_{i-1/2})^2, 0)^T, \check{s}^-_{i-1/2}\}, \tag{35a}$$

$$\{w^2_{i-1/2}, s^2_{i-1/2}\} = \{(0, 0, 1, 0)^T, \frac{1}{2}(\check{s}^-_{i-1/2} + \check{s}^+_{i-1/2})\}, \tag{35b}$$

$$\{w^3_{i-1/2}, s^3_{i-1/2}\} = \{(1, \check{s}^+_{i-1/2}, (\check{s}^+_{i-1/2})^2, 0)^T, \check{s}^+_{i-1/2}\}. \tag{35c}$$

We will consider $\{w^0_{i-1/2}, s^0_{i-1/2}\}$, and how it affects the solution, below in Section 4.2.1.

The system (31) is over-determined in that it contains a redundant equation for φ, since φ is only a function of h and hu. Therefore, the physical relevance of the form of $r^2(\tilde{q})$ and $\lambda^2(\tilde{q})$ in (34) is not clear since this field can carry variation only in the third component, the momentum flux φ, which is a function only of h and hu. Including a wave representing this field in our approximate Riemann solution allows an extra degree of freedom for φ, which is warranted since the change in h, hu and φ across a single discontinuity is typically inconsistent with the true smooth rarefaction wave in the exact Riemann solution. In the future we wish to explore connections between using this additional wave and relaxation solvers, such as described in [30,22]. We return to the corrector wave $w^2_{i-1/2}$ in Section 5. In the next section we discuss the stationary wave $w^0_{i-1/2}$.

4.2.1. The steady state wave

By incorporating the bottom surface $b(x)$ as an additional solution variable in $\tilde{q}$, the shallow water equations have been written as a homogeneous system (31) with no source term. This introduces a new linearly degenerate field with an identically zero eigenvalue $\lambda^0(\tilde{q}) \equiv 0$. Variation in $b(x)$ occurs entirely with respect to this field. In fact, this field carries the variation of all the components of $\tilde{q}$ for a smooth steady state, since a non-trivial steady state solution to (31) satisfies

$$W(\tilde{q})\tilde{q}_x = 0, \tag{36}$$

which implies that $\tilde{q}_x$ is proportional to $r^0(\tilde{q})$. That is, smooth steady state solutions $\tilde{q}(x, \cdot)$ are integral curves of $r^0(\tilde{q})$ in $\mathbb{R}^4$, parameterized by x.

For the approximate solver defined by (29) the pair $\{w^0_{i-1/2}, s^0_{i-1/2}\}$ is chosen to be an approximation to $r^0(\tilde{q})$ and $\lambda^0(q)$ based on the local solution. Since $s^0_{i-1/2} = \lambda^0(\tilde{q}) = 0$, the resulting stationary wave in the approximate Riemann solution is a jump discontinuity remaining at the cell interface, which contributes the effect of the source term. By defining the vector $w^0_{i-1/2}$ in the right way using special averages of the two states Q_i and Q_{i-1}, we believe that the solver preserves a larger class of steady states than has been accomplished before in a simple solver framework. This is described below. Some other approximate solvers that have a stationary discontinuity at the cell interface due to a source term can be found in [3,11].

For any two states, we define two different averages for $\lambda^+(q)\lambda^-(q) = u^2 - gh$, the product of the shallow water eigenvalues. We write these averages as functions of Q_i and Q_{i-1}, and denote them with a bar and tilde,

$$\overline{\lambda^+\lambda^-}(Q_{i-1}, Q_i) = \left(\frac{U_{i-1} + U_i}{2}\right)^2 - g\left(\frac{H_{i-1} + H_i}{2}\right), \tag{37}$$

and

$$\widetilde{\lambda^+\lambda^-}(Q_{i-1}, Q_i) = \max(0, U_i U_{i-1}) - g\left(\frac{H_{i-1} + H_i}{2}\right). \tag{38}$$

We also define two average depths, the simple arithmetic average

$$\overline{H}(Q_{i-1}, Q_i) = \left(\frac{H_{i-1} + H_i}{2}\right), \tag{39}$$

and

$$\widetilde{H}(Q_{i-1}, Q_i) = \overline{H}(Q_{i-1}, Q_i)\frac{\widetilde{\lambda^+\lambda^-}(Q_{i-1}, Q_i)}{\overline{\lambda^+\lambda^-}(Q_{i-1}, Q_i)}. \tag{40}$$

We then let

$$w^0_{i-1/2} = \begin{bmatrix} \frac{g\overline{H}(Q_{i-1}, Q_i)}{\overline{\lambda^+\lambda^-}(Q_{i-1}, Q_i)} \\ 0 \\ -g\widetilde{H}(Q_{i-1}, Q_i) \\ 1 \end{bmatrix}. \tag{41}$$

Note that (41) resembles $r^0(\tilde{q})$, evaluated with special averages of the left and right states. The form of the averages used in the vector (41) is due to the following fact, which we write as a theorem:

Theorem 1. *Suppose that a smooth steady state solution to the shallow water equations exists between two points, x_l and x_r, with $b(x_l) \neq b(x_r)$. If the vector $\tilde{q}(x,t) \in \mathbb{R}^4$ is differenced between x_l and x_r, then the difference satisfies*

$$\tilde{q}(x_r, t) - \tilde{q}(x_l, t) = (b(x_r) - b(x_l)) \begin{bmatrix} \frac{g\overline{H}(q(x_l,t), q(x_r,t))}{\overline{\lambda^+\lambda^-}(q(x_l,t), q(x_r,t))} \\ 0 \\ -g\widetilde{H}(q(x_l,t), q(x_r,t)) \\ 1 \end{bmatrix}. \tag{42}$$

Proving (42) involves well known properties of steady state solutions, and is left to Appendix A. Theorem 1 implies that if the numerical data, $\widetilde{Q}_i = (H_i, HU_i, \varphi(Q_i), B_i)^T$ and $\widetilde{Q}_{i-1} = (H_{i-1}, HU_{i-1}, \varphi(Q_{i-1}), B_{i-1})^T$ correspond to evaluating a smooth steady state at two points surrounding variable bathymetry, then the decomposition (29) will have only one non-zero wave—the *steady state wave*—since

$$\widetilde{Q}_i - \widetilde{Q}_{i-1} = \alpha^0_{i-1/2} w^0_{i-1/2} = (B_i - B_{i-1}) w^0_{i-1/2}. \tag{43}$$

Since the steady state wave is stationary the discrete steady state will be exactly maintained as a jump discontinuity at the cell interface $x_{i-1/2}$. Theorem 1 or Eq. (43) imply that if we choose any two points, say $\widetilde{Q}_i \in \mathbb{R}^4$ and $\widetilde{Q}_{i-1} \in \mathbb{R}^4$, lying on an integral curve of $r^0(\tilde{q}) \in \mathbb{R}^4$, those points will be connected by the vector $(B_i - B_{i-1}) w^0_{i-1/2}$. We will refer to such a pair of states, $\widetilde{Q}_i$ and $\widetilde{Q}_{i-1}$, as *steady state data*.

Additionally, it is easy to show that the motionless steady state, $(h+b)_x \equiv 0$, $hu \equiv 0$, satisfies (42) regardless of the smoothness of the depth h and the underlying bathymetry b, and therefore numerical data $H_i + B_i = H_{i-1} + B_{i-1}$, $U_i = U_{i-1} = 0$, satisfies (43). These properties obviously allow convergence to smooth steady states, but more importantly allow perfect maintenance of discrete steady states, even on coarse grids.

For Riemann data not satisfying (43), the decomposition (29) will generate propagating waves. The waves $\mathcal{Z}^p_{i-1/2}$ for $p \neq 0$, represent deviations to the steady state which propagate away from the cell interface, and the two states remaining on either side of the cell interface are approximately steady state data. For certain exceptional non-steady state Riemann problems, the definitions in (41) might become problematic if either $\lambda^+\lambda^-$ or $\overline{\lambda^+\lambda^-}$ approach zero. This is related to the loss of hyperbolicity of (31), which occurs when one of the eigenvalues passes through zero. We wish to explore this topic further in the future. Numerically this problem can be circumvented by imposing bounds on $(w^0_{i-1/2})^1$ and $(w^0_{i-1/2})^3$. We address such bounds in the following sections when we discuss consistency and preserving depth non-negativity in the presence of a source term.

4.2.2. Consistency of the steady state wave and the source term

A discontinuity proportional to (41) at the cell interface acts as a source of momentum, as can be seen by considering the updating fluctuations, defined by (23). Note that the stationary wave $\mathcal{Z}^0_{i-1/2}$ is not included in $\mathcal{A}^{\pm}\Delta Q_{i-1/2}$ since this wave does not move into either adjacent grid cell. Therefore, the decomposition (29) defines exactly the same fluctuations as would be obtained by first subtracting the stationary wave from the Riemann data:

$$\begin{bmatrix} H_i - H_{i-1} \\ HU_i - HU_{i-1} \\ \varphi(Q_i) - \varphi(Q_{i-1}) \\ B_i - B_{i-1} \end{bmatrix} - \alpha^0_{i-1/2} w^0_{i-1/2} = \sum_{p=1}^{3} \alpha^p_{i-1/2} w^p_{i-1/2}. \tag{44}$$

Since only $w^0_{i-1/2}$ has a non-zero fourth component, we know that $\alpha^0_{i-1/2} = (B_i - B_{i-1})$. Therefore, Eq. (44) corresponds to the following decomposition of the momentum flux

$$\varphi(Q_i) - \varphi(Q_{i-1}) - (-g\widetilde{H}(Q_{i-1}, Q_i)(B_i - B_{i-1})) = \sum_{p=1}^{3} (\alpha^p_{i-1/2} w^p_{i-1/2})^3. \tag{45}$$

Eq. (45) represents subtracting an approximation to the source term (integrated over a cell length) from the momentum flux. This is exactly what is advocated in [3]. However, in [3], it is not determined what the best form of the source term approximation should be given the initial Riemann data (*i.e.* what average of the initial depths H_i and H_{i-1} should be used in $-ghb_x$). By using $-g\widetilde{H}(Q_{i-1}, Q_i)$ to approximate $-gh$, we are able to precisely preserve smooth steady states over variable bathymetry. That is,

$$-g\widetilde{H}(q(x_l, t), q(x_r, t))(b(x_r) - b(x_l)) = -\int_{x_l}^{x_r} ghb_x \, \mathrm{d}x \tag{46}$$

is exactly satisfied for such solutions, as long as $b(x_r) - b(x_l) \neq 0$ (see Appendix A or [14]).

For problems that are far from a steady state it is reasonable to impose a bound on $\widetilde{H}(Q_{i-1}, Q_i)$ for consistency and stability. Since it is an approximation to the depth, a suitable set of bounds might be

$$\min(H_i, H_{i-1}) \leqslant \widetilde{H}(Q_{i-1}, Q_i) \leqslant \max(H_i, H_{i-1}). \tag{47}$$

One may choose other bounds based on the initial Riemann data or the approximate solution as well. For Riemann problems that are a discretization of smooth steady state data, it is easy (at least for monotonically varying bathymetry) to show that (47) is automatically satisfied (see [14]). In our simulations we impose (47).

4.2.3. Preserving depth non-negativity with a source term

When variable bathymetry is introduced into the Riemann problem a stationary discontinuity in depth is introduced into the Riemann solution at the cell interface, due to the first component of $w^0_{i-1/2}$. The net sum of the mass to both sides of this interface remains positive, due to mass conservation and the depth positive semi-definite feature for the homogeneous problem discussed at the end of Section 4.1. However, it is possible that the jump discontinuity produces a positive depth to one side of the interface and a negative depth to the other. This does not occur for steady state problems (see [14]), and it can be prevented for other problems by imposing bounds on the jump in depth h at this interface, or equivalently, bounding the first component of $w^0_{i-1/2}$. It

can be shown (see [14]) that for subcritical flow the following bounds prevent negativity of the depth in the approximate solution

$$\frac{(\check{s}^+_{i-1/2} - \check{s}^-_{i-1/2})}{\check{s}^-_{i-1/2}} \frac{\check{H}^*_{i-1/2}}{(B_i - B_{i-1})} \leqslant (w^0_{i-1/2})^1 \leqslant -1 \quad \text{if } B_i - B_{i-1} > 0, \tag{48}$$

$$\frac{(\check{s}^+_{i-1/2} - \check{s}^-_{i-1/2})}{\check{s}^+_{i-1/2}} \frac{\check{H}^*_{i-1/2}}{(B_i - B_{i-1})} \leqslant (w^0_{i-1/2})^1 \leqslant -1 \quad \text{if } B_i - B_{i-1} < 0, \tag{49}$$

where $\check{H}^*_{i-1/2}$ is the single middle state depth of the HLLE solver given by (28).

For supercritical flow $\left(w^0_{i-1/2}\right)^1$ is positive. Bounds on $(w^0_{i-1/2})^1$ are not necessary due to mass conservation and the net summation of waves moving in one direction, but a bound that preserves depth non-negativity between each wave of the approximate solution can be easily derived, and might provide more accurate second order correction terms. For transcritical Riemann problems where $B_i \neq B_{i-1}$, we set $(w^0_{i-1/2})^1 = 0$ to avoid possible instabilities. This type of Riemannn problem is physically dubious, but might arise numerically near extrema in $b(x)$ or near stationary shocks. See [14] for a discussion. We plan to study these issues for transcritical and supercritical Riemann problems further in the future.

4.3. Second order correction terms

4.3.1. Maintaining steady state preservation

The first order wave propagation method using the Riemann solver described above is well-balanced in the sense that it perfectly preserves a sequence of solution data, $\{\ldots, Q_{i-1}, Q_i, Q_{i+1}, \ldots\}$, if each adjacent pair of states is steady state data (*i.e.* satisfies (43)). The correction terms $\widetilde{F}_{i\pm1/2}$ must also preserve the same steady state data (*i.e.* contribute no update). This is satisfied by using (17) for the correction terms: since the steady state wave has $\operatorname{sgn}(s^0_{i-1/2}) = 0$, it does not affect $\widetilde{F}_{i-1/2}$, which for steady state data is given by

$$\widetilde{F}_{i-1/2} = \frac{1}{2}\operatorname{sgn}(s^0_{i-1/2})\left(1 - \frac{\Delta t}{\Delta x}|s^0_{i-1/2}|\right)\widetilde{\mathcal{Z}}^0_{i-1/2} = 0. \tag{50}$$

4.3.2. Limiting the correction terms to preserve positivity

Correction terms can also contribute to a spurious negative depth in the numerical solution, even if the first order method (6) preserves the depth non-negativity of the solution. However, by using a simple additional limiting strategy on the fluxes $\widetilde{F}_{i\pm1/2}$, it is possible to prevent this effect. See [14] for details, and extension to the two-dimensional problem.

5. Improving accuracy for shorelines and rarefactions

In this section we will be discussing some properties of exact Riemann solutions to the original homogeneous shallow water Eqs. (20), which contain two fields defined by (24). Recall that the first wave $\mathcal{Z}^1_{i-1/2}$ in our approximate Riemann solution is related to $\{r^1(\tilde{q}), \lambda^1(\tilde{q})\}$ of (34), which corresponds to the first-field of the shallow water equations—defined by $\{r^-(q), \lambda^-(q)\}$ in (24). Regrettably, a possible source of confusion is that the third wave $\mathcal{Z}^3_{i-1/2}$, related to $\{r^3(\tilde{q}), \lambda^3(\tilde{q})\}$ of (34), corresponds to the *second*-field of the shallow water equations, defined by $\{r^+(q), \lambda^+(q)\}$ in (24). Below we show how $\mathcal{Z}^2_{i-1/2}$ can be used to complement $\mathcal{Z}^1_{i-1/2}$ or $\mathcal{Z}^3_{i-1/2}$, providing a better approximation to the exact Riemann solution when it contains a large rarefaction. We will also modify and generalize the definition of the Einfeldt speeds (26), allowing a better approximation to Riemann problems with an initial dry state, or near-dry state.

For the shallow water equations, the structure of the exact Riemann solution can be determined (*i.e.* whether the wave in each field is a shock or rarefaction) by a single function evaluation using the initial Riemann data (see Appendix B). Using this, we can classify the Riemann solution as belonging to one of four types: type-one, both fields have a shock; type-two, one field has a shock and the other a rarefaction; type-three, both fields have a rarefaction; or type-four, one state is initially dry, so only one wave is defined and

is a rarefaction. Given the structure of the Riemann solution, in some situations we will determine or approximate the depth of the middle state—the constant solution in the region between the propagating waves in the exact Riemann solution. We will denote the middle state with a star: $Q^*_{i-1/2}$ (see Fig. 1).

5.1. Riemann problems with strong or transonic rarefactions

As explained in Section 4.1, we expect that $\mathcal{Z}^2_{i-1/2}$ will be small in magnitude for Riemann problems without a significant or *strong* rarefaction in one field. For such problems, we use $w^2_{i-1/2} = (0, 0, 1, 0)^T$ since this provides linearly independent vectors and results in a mass update that corresponds to the depth positive semi-definite HLLE solver. For problems with a large rarefaction in one field, particularly a transonic rarefaction, an alternative definition of the pair $\{w^2_{i-1/2}, s^2_{i-1/2}\}$ allows a more accurate approximate Riemann solution. Fig. 1 depicts these types of Riemann problems. Given a large rarefaction in the first field, we might use $\{w^1_{i-1/2}, s^1_{i-1/2}\}$ and $\{w^2_{i-1/2}, s^2_{i-1/2}\}$ to approximate $\{r^1(\tilde{q}), \lambda^1(\tilde{q})\}$ at the left and right edges of the rarefaction (see Fig. 1(a)), or given a large rarefaction in the second field, we might use $\{w^2_{i-1/2}, s^2_{i-1/2}\}$ and $\{w^3_{i-1/2}, s^3_{i-1/2}\}$ to approximate $\{r^3(\tilde{q}), \lambda^3(\tilde{q})\}$ at the left and right edges of the rarefaction (see Fig. 1(b)). Neither $\{w^1_{i-1/2}, s^1_{i-1/2}\}$ or $\{w^3_{i-1/2}, s^3_{i-1/2}\}$ needs to be modified, since, given a rarefaction in the first or second field respectively, by using the Einfeldt speeds, $\{w^1_{i-1/2}, s^1_{i-1/2}\}$ already corresponds to evaluating $\{r^1(\tilde{q}), \lambda^1(\tilde{q})\}$ at the left state Q_{i-1}, and $\{w^3_{i-1/2}, s^3_{i-1/2}\}$ corresponds to evaluating $\{r^3(\tilde{q}), \lambda^3(\tilde{q})\}$ at the right state Q_i. Since $r^{\pm}(q)$ is only a function of its respective eigenvalue $\lambda^{\pm}(q)$, to build $\{w^2_{i-1/2}, s^2_{i-1/2}\}$ we only need an approximation to $\lambda^-(Q^*_{i-1/2})$ in the event of a large 1-rarefaction or $\lambda^+(Q^*_{i-1/2})$ for a large 2-rarefaction. Using the Riemann invariants of each characteristic field, it is easily shown that for a rarefaction in the first characteristic field,

$$\lambda^-(Q^*_{i-1/2}) = U_{i-1} + 2\sqrt{gH_{i-1}} - 3\sqrt{gH^*_{i-1/2}}, \tag{51a}$$

and for a rarefaction in the second characteristic field,

$$\lambda^+(Q^*_{i-1/2}) = U_i - 2\sqrt{gH_i} + 3\sqrt{gH^*_{i-1/2}}. \tag{51b}$$

We therefore only require an approximation to the middle state depth $H^*_{i-1/2}$, which is easily accomplished (see Appendix B). The speeds (51) also provide an indication of the strength of a given rarefaction, and whether it is transonic.

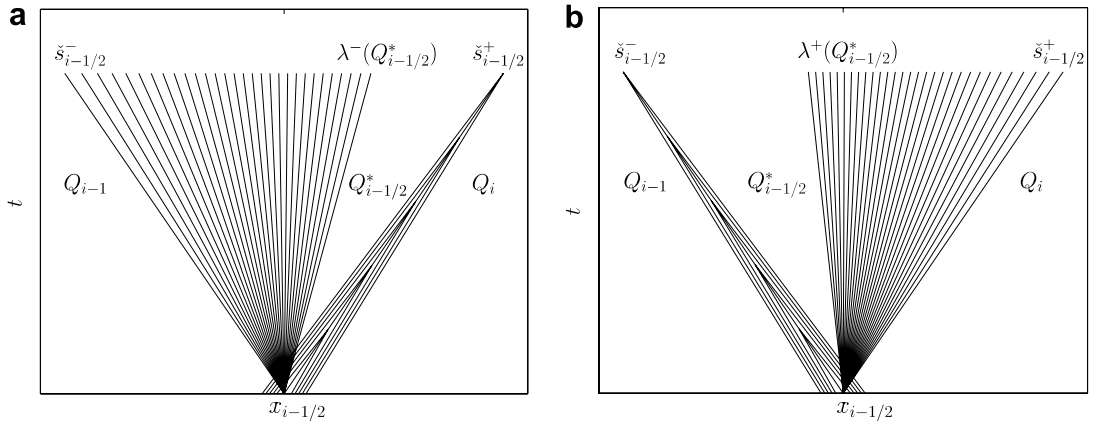

Fig. 1. Riemann problems with a large rarefaction in one characteristic family and a shock in the other. Characteristics of each family are shown through the respective wave in that family. (a) A Riemann problem with a large transonic rarefaction in the first field. The Riemann problem is approximated by three discontinuities moving with speeds $s^1_{i-1/2} = \check{s}^-_{i-1/2}$, $s^2_{i-1/2} \approx \lambda^-(Q^*_{i-1/2})$ and $s^3_{i-1/2} = \check{s}^+_{i-1/2}$. (b) A Riemann problem with a large transonic rarefaction in the second field. The Riemann problem is approximated by three discontinuities moving with speeds $s^1_{i-1/2} = \check{s}^-_{i-1/2}$, $s^2_{i-1/2} \approx \lambda^+(Q^*_{i-1/2})$ and $s^3_{i-1/2} = \check{s}^+_{i-1/2}$. In both cases two of the discontinuities are used to approximate the large rarefaction and the other approximates the shock.

For any Riemann problem, we will define the following speeds as functions of $H^*_{i-1/2}$ (whether $H^*_{i-1/2}$ is exact or only an approximation to the middle state depth):

$$\lambda^{-*}_{i-1/2}(H^*_{i-1/2}) = U_{i-1} + 2\sqrt{gH_{i-1}} - 3\sqrt{gH^*_{i-1/2}}, \tag{52a}$$

$$\lambda^{+*}_{i-1/2}(H^*_{i-1/2}) = U_i - 2\sqrt{gH_i} + 3\sqrt{gH^*_{i-1/2}}. \tag{52b}$$

We now let

$$\{w^2_{i-1/2}, s^2_{i-1/2}\} = \left\{\left(1, \lambda^{-*}_{i-1/2}(H^*_{i-1/2}), (\lambda^{-*}_{i-1/2}(H^*_{i-1/2}))^2, 0\right)^T, \lambda^{-*}_{i-1/2}(H^*_{i-1/2})\right\}, \tag{53a}$$

in the event of a strong 1-rarefaction, and

$$\{w^2_{i-1/2}, s^2_{i-1/2}\} = \{(1, \lambda^{+*}_{i-1/2}(H^*_{i-1/2}), (\lambda^{+*}_{i-1/2}(H^*_{i-1/2}))^2, 0)^T, \lambda^{+*}_{i-1/2}(H^*_{i-1/2})\}, \tag{53b}$$

in the event of a strong 2-rarefaction.

In shallow regions $H^*_{i-1/2}$ might get small. As $H^*_{i-1/2}$ approaches zero the second pair $\{w^2_{i-1/2}, s^2_{i-1/2}\}$ should again be defined by (35b), so that the Riemann solver is guaranteed to be depth positive semidefinite. In the next section we cover dry-state Riemann problems.

5.2. Dry-state Riemann problems

For Riemann problems with an initial dry state to one side, the exact Riemann solution contains only a single rarefaction connecting the wet to the dry state (see *e.g.* [37]). The evolving wet–dry interface is therefore simply one edge of the rarefaction. The propagation speed of this interface can be exactly determined using the Riemann invariants of the corresponding characteristic field. If the left state is initially dry, the rarefaction is in the second characteristic field, and the wet–dry interface propagates at a speed

$$U_i - 2\sqrt{gH_i}. \tag{54a}$$

For an initially dry right state, the rarefaction is in the first characteristic field, and the wet–dry interface propagates at a speed

$$U_{i-1} + 2\sqrt{gH_{i-1}}. \tag{54b}$$

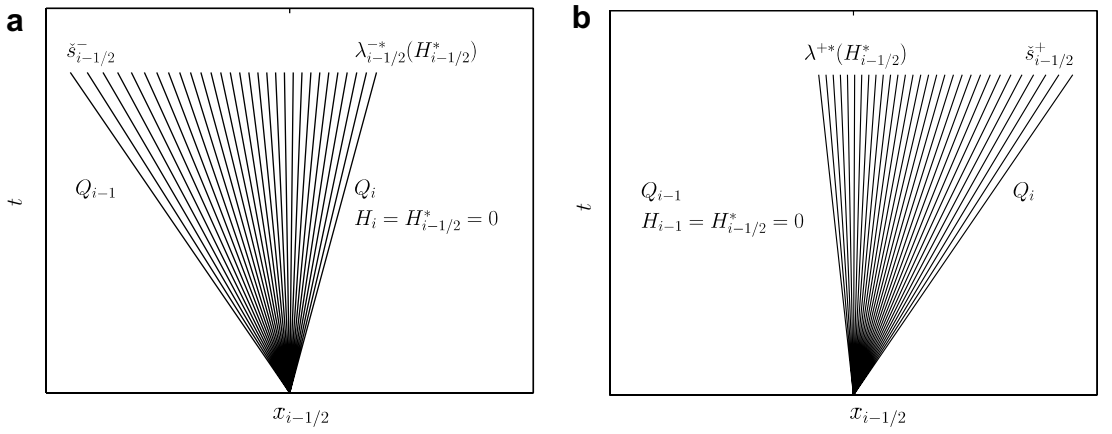

Fig. 2. The initial dry bed Riemann problems in the x–t plane. (a) The single rarefaction in the first field when $H_i = 0$. The wet–dry interface moves with speed $s^3_{i-1/2} = \check{s}^+_{i-1/2} = \lambda^{-*}_{i-1/2}(0) = U_{i-1} + 2\sqrt{gH_{i-1}}$. (b) The single rarefaction in the second field when $H_{i-1} = 0$. The wet–dry interface moves with speed $s^1_{i-1/2} = \check{s}^-_{i-1/2} = \lambda^{+*}_{i-1/2}(0) = U_i - 2\sqrt{gH_i}$.

The speeds (54) correspond exactly to (52), since, in this case, the "middle state depth" $H^*_{i-1/2}$, corresponds to the initial dry state and is therefore zero. See Fig. 2, which depicts this characteristic structure of the two dry state Riemann problems.

Another interpretation of Riemann problems with an initial dry state is that waves in both fields still exist but the wave in one field has zero strength. In this case, the wet–dry interface actually corresponds to an overlapping of the edge of a rarefaction in one field, and a zero strength shock in the other field moving at the same speed. In fact, for Riemann problems in which both states are wet, but one is vanishingly small, the speed of the edge of the rarefaction in one field approaches the speed of the wave in the other field. The dry state Riemann solution might be thought of as the limit of this process. Therefore, for dry state problems we can still always interpret $\{w^1_{i-1/2}, s^1_{i-1/2}\}$ as being an approximation to the first field of the shallow water equations and $\{w^3_{i-1/2}, s^3_{i-1/2}\}$ an approximation to the second field, even though we want the pairs $\{w^1_{i-1/2}, s^1_{i-1/2}\}$ and $\{w^3_{i-1/2}, s^3_{i-1/2}\}$ to be approximations to the eigenpair of the field containing the rarefaction, at the two edges of the rarefaction. This can be accomplished by adjusting the Einfeldt speeds (26) in the case of an initial dry state, and then continuing to use the same definition for $\{w^1_{i-1/2}, s^1_{i-1/2}\}$ and $\{w^3_{i-1/2}, s^3_{i-1/2}\}$. That is, we define the speeds

$$\check{s}^-_{i-1/2} = \min(\hat{\lambda}^-_{i-1/2}, \lambda^-(Q_{i-1})) = \lambda^-(Q_{i-1}) = U_{i-1} - \sqrt{gH_{i-1}}, \tag{55a}$$

$$\check{s}^+_{i-1/2} = \lambda^{-*}(H^*_{i-1/2}) = U_{i-1} + 2\sqrt{gH_{i-1}}, \tag{55b}$$

when the right state is initially dry ($H_i = 0$), and

$$\check{s}^-_{i-1/2} = \lambda^{+*}(H^*_{i-1/2}) = U_i - 2\sqrt{gH_i}, \tag{56a}$$

$$\check{s}^+_{i-1/2} = \max(\hat{\lambda}^+_{i-1/2}, \lambda^+(Q^*_{i-1/2})) = \lambda^+(Q^*_{i-1/2}) = U_i + \sqrt{gH_i}, \tag{56b}$$

when the left state is initially dry ($H_{i-1} = 0$). In each case, only one of the Einfeldt speeds has been modified to reflect the speed of the wet dry interface, and the other unchanged Einfeldt speed corresponds to the speed of the rarefaction adjacent to the initial wet state (as can easily be shown by calculating the Roe speed). See Fig. 2.

In the next section we will show how we can generalize the Einfeldt speeds, so that they better reflect the true wave speeds as well as approach (55) or (56) as H_i or H_{i-1} approaches zero.

For many dry state Riemann problems over variable topography, the source term must typically be adjusted for most schemes, since a discretization of $-ghb_x$ involves the difference $B_i - B_{i-1}$, which is physically irrelevant if B_i or B_{i-1} is much greater than the water level. (Such as would occur at a steep shoreline.) See, for instance, [2]. The approach we take is to solve a homogeneous Riemann problem to determine the relevant value of B_i or B_{i-1} when $H_i = 0$ or $H_{i-1} = 0$ respectively. For instance, if $H_i = 0$ and $H_{i-1} + B_{i-1} < B_i$, we first solve the homogeneous Riemann problem with ghost values in cell $\mathcal{C}_i$: $B_i = B_{i-1}$, $H_i = H_{i-1}$ and $HU_i = -HU_{i-1}$, which simulates a wall boundary condition. The resulting middle state solution ($H^*_{i-1/2}$) to the homogeneous problem determines the maximum height that water in cell $\mathcal{C}_{i-1}$ would rise up a wall. The original Riemann problem is then solved as a normal dry state Riemann problem with B_i replaced by $\max(B_i, H^*_{i-1/2} + B_{i-1})$. The analogous procedure is taken when the left state is dry and $B_{i-1} > H_{i-1} + B_{i-1}$.

5.3. Generalization of the Einfeldt speeds and implementation

For exact Riemann solutions, the wave (whether a rarefaction or shock) in one field never surpasses the characteristics in the other field—waves in the first field are never greater in speed than waves in the second (see *e.g.* [27]). For dry state problems, the wave in one field becomes as fast as the wave in the other field, so we have let $\check{s}^-_{i-1/2} = \lambda^{+*}_{i-1/2}$ when $H_{i-1} = 0$ or $\check{s}^+_{i-1/2} = \lambda^{-*}_{i-1/2}$ when $H_i = 0$. However, for problems near a dry state, it is possible that our speed estimates are such that $\check{s}^+_{i-1/2} < \lambda^{-*}_{i-1/2}$ when H_i is very small, or $\lambda^{+*}_{i-1/2} < \check{s}^-_{i-1/2}$ when H_{i-1} is small. We therefore redefine the Einfeldt speeds, for all Riemann problems, by

$$\check{s}^-_{i-1/2} = \min(\lambda^-(Q_{i-1}), \hat{\lambda}^-_{i-1/2}, \lambda^{+*}_{i-1/2}(H^*_{i-1/2})), \tag{57a}$$

$$\check{s}^+_{i-1/2} = \max(\lambda^+(Q_i), \hat{\lambda}^+_{i-1/2}, \lambda^{-*}_{i-1/2}(H^*_{i-1/2})) \tag{57b}$$

recognizing that these speeds still usually correspond to one of the first two arguments in the min or max, as depicted in Fig. 1. (By using the secant estimate for $H^*_{i-1/2}$ described in Appendix B, it can be shown that $\lambda^{-*}(H^*_{i-1/2})$ is never actually greater than the speed of a true shock in the second characteristic family, and $\lambda^{+*}(H^*_{i-1/2})$ is never actually less than the speed of a true shock in the first family (see [14]). The inclusion of $\lambda^{\mp*}(H^*_{i-1/2})$ in the definition of our speeds $\check{s}^{\pm}_{i-1/2}$ in (57) is therefore never unjustified with respect to the true Riemann structure.) Another advantage to using (57) is that it corresponds to (55) and (56) if one state is dry by simply omitting the speeds that are undefined in each case. That is, if $H_i = 0$, then U_i is undefined and the quantities $\lambda^+(Q_i)$ and $\lambda^{+*}_{i-1/2}(H^*_{i-1/2})$ are omitted from (57). If $H_{i-1} = 0$, then U_{i-1} is undefined and the quantities $\lambda^-(Q_{i-1})$ and $\lambda^{-*}_{i-1/2}(H^*_{i-1/2})$ are omitted from (57). By a simple calculation of the Roe speeds, it can easily be shown that the speeds (57) then correspond to (55) when the right state is initially dry ($H_i = 0$), and correspond to (56) when the left state is initially dry($H_{i-1} = 0$).

In summary, to implement the modifications described in this section, the only added complexity to the original solver is the estimation of $H^*_{i-1/2}$ and establishing some criteria that determines if the alternative form of $\{w^2_{i-1/2}, s^2_{i-1/2}\}$ should be used for a given Riemann problem. The latter can be based on the value of $H^*_{i-1/2}$ compared to the initial data H_i and H_{i-1}. For problems with a large rarefaction, $H^*_{i-1/2} << \max(H_i, H_{i-1})$, indicating a rarefaction in one field. In this case, the alternative form for $\{w^2_{i-1/2}, s^2_{i-1/2}\}$ might provide a better approximate Riemann solution. In shallow regions, where $H^*_{i-1/2}$ approaches zero and $s^2_{i-1/2}$ approaches $s^1_{i-1/2}$ or $s^3_{i-1/2}$, the original form for $\{w^2_{i-1/2}, s^2_{i-1/2}\}$ should be resorted to, providing depth non-negativity and linearly independence of the vectors $w^p_{i-1/2}$. In all cases $\{w^1_{i-1/2}, s^1_{i-1/2}\}$ and $\{w^3_{i-1/2}, s^3_{i-1/2}\}$ are defined by (35) using the generalized Einfeldt speeds (57) (assuming undefined speeds are omitted given an initial dry state).

6. Numerical tests and results

The Riemann solver described in this paper provides a set of waves and fluctuations necessary for the high-resolution (second-order) wave propagation method, given by (7). For additional details on implementing the wave propagation method (for instance the use of correction terms and limiters), see [27,25,14]. In the figures and references in this section we will refer to our algorithm as the 'A4WS' method, for *Augmented 4-Wave Solver*, since it is based on an augmented system—equations (31). Below we show some numerical results using our method for several one-dimensional test cases. The first two problems are chosen for the sake of comparison to other algorithms since these problems have been commonly applied and test maintenance of steady state flow over a hump. Finally, we introduce a one-dimensional problem to test tsunami propagation and inundation. See [15,29,14,16] for some two-dimensional tsunami simulations with adaptive mesh refinement using extensions of the algorithms presented here.

6.1. Subcritical steady flow

This first problem tests convergence to subcritical flow over a hump, and is borrowed from [8]. The domain, boundary and initial conditions are

$$h(x,0) = 2.0 - b(x), \quad hu(x,0) \equiv 4.42, \quad 0 \leqslant x \leqslant 25, \tag{58}$$

$$hu(0,t) = 4.42, \quad h(25,t) = 2.0, \quad 0 \leqslant t \leqslant 200 \tag{59}$$

and the bottom topography is given by

$$b(x) = \begin{cases} 0.2 - 0.05(x-10)^2 & \text{if } 8 < x < 12, \\ 0 & \text{otherwise.} \end{cases} \tag{60}$$

We computed this problem using 200 grid points, as in [8], and with 50 grid points. Fig. 3 shows the numerical solution at $t = 200$ using the A4WS method. The goal of the problem is to investigate convergence to a non-stationary steady state. With older schemes based on traditional Riemann solvers and fractional stepping, spurious oscillations would typically appear near steep gradients in the bathymetry. See, for instance, the papers [3,26]. Convergence to the steady state without oscillations is most easily judged by observing the momentum hu, which should be constant. Table 1 shows the l_∞ error for hu for the subcritical flow over a hump problem,

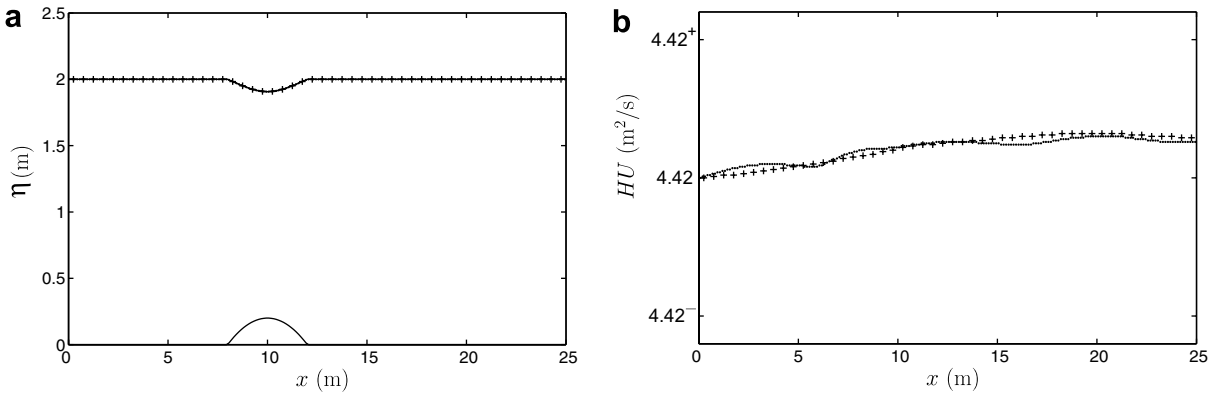

Fig. 3. Subcritical steady flow over a hump. A4WS numerical solution at $t = 200$. (a) Surface elevation ($\eta(x, 200) = H(x, 200) + B(x)$) computed with 200 grid points (·) and 50 grid points (+). Bathymetry is shown as a solid line. (b) Close-up of the momentum HU computed with 200 points (·) and 50 points (+). The true steady state solution is a constant $hu \equiv 4.42$. To show the error, the vertical axis scale is greatly magnified: $4.42^{\pm} = 4.42 \pm 10^{-5}$.

Table 1
The l_∞ error for hu for the A4WS method is compared to the relaxation method described in [8] using 200 grid points

Method	l_∞ error for hu	$(l_\infty$ error for $hu)/h$	$(l_\infty$ error for $hu)/\Delta x$
A4WS	3.0×10^{-6}	1.5×10^{-6}	2.4×10^{-5}
Relaxation [8]	$\approx 5.0 \times 10^{-3}$	$\approx 2.5 \times 10^{-3}$	$\approx 4.0 \times 10^{-2}$
A4WS (50 points)	3.2×10^{-6}	1.6×10^{-6}	6.4×10^{-6}

The A4WS error using 50 points is also shown.

comparing the A4WS method to the relaxation method described in [8], indicating the degree to which the steady state is maintained. (The error for the relaxation method is interpreted from figures in [8], and is therefore only roughly approximate.) Since maintenance of the steady state at any given grid resolution is an important property of tsunami modeling, we also computed the problem using 50 grid points to test the accuracy of steady state maintenance even on very coarse grids.

6.2. Transcritical steady flow with a shock

This one-dimensional test, borrowed from [4], was originally computed in [18] and later discussed in [11]. The domain, boundary and initial conditions are

$$h(x, 0) \equiv 0.33, \quad hu(x, 0) \equiv 0.18, \quad 0 \leqslant x \leqslant 25, \tag{61}$$

$$hu(0, t) = 0.18, \quad h(25, t) = 0.33, \quad 0 \leqslant t \leqslant 200 \tag{62}$$

and the bottom topography is again given by

$$b(x) = \begin{cases} 0.2 - 0.05(x - 10)^2 & \text{if } 8 < x < 12, \\ 0 & \text{otherwise.} \end{cases} \tag{63}$$

The eventual steady state solution contains a critical point and stationary shock. (Stationary and slow moving shocks are notorious for generating spurious oscillations, even for shock-capturing schemes [1,23].) Fig. 4 shows the solution for this test problem, at $t = 200$, using 200 and 50 grid points. The steady state should have hu constant throughout the domain, even through the shock (though the exact solution does not appear to have completely reached steady state to the right of the shock at $t = 200$). The A4WS method maintains the smooth steady state without oscillations even on the very coarse grid using 50 points, presumably due to the form of the steady state wave $w^0_{i-1/2}$. (While maintaining the steady state

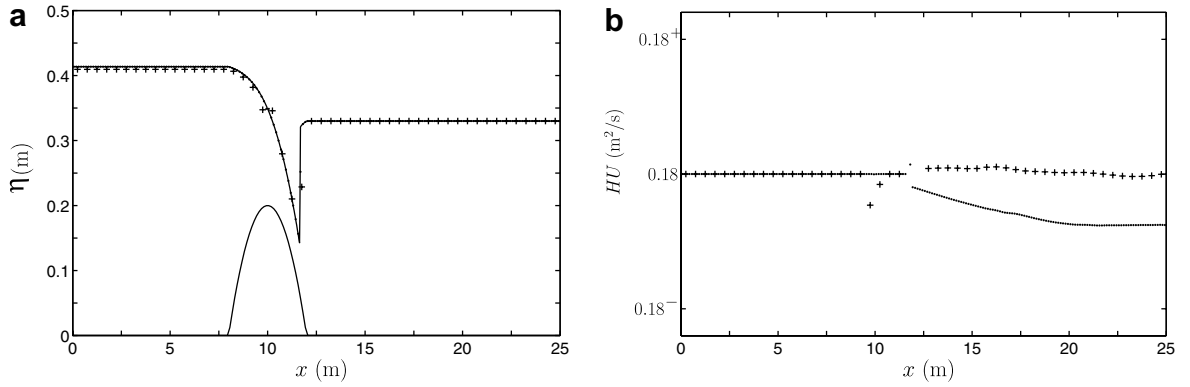

Fig. 4. Transcritical flow with a shock. A4WS numerical solution at $t = 200$. (a) The surface elevation $\eta(x, 200) = H(x, 200) + B(x)$ computed with 200 points (·) and 50 points (+). Reference solution (computed with 2000 points) and bathymetry are shown as solid lines. Spurious oscillations are absent near the stationary shock or rapidly varying bottom surface. (b) Close-up of the momentum HU computed with 200 points (·) and 50 points (+). The true steady state solution should be constant $hu \equiv 0.18$. The vertical axis is greatly magnified: $0.18^{\pm} = 0.18 \pm 10^{-4}$.

does not appear to require a fine grid, the surface elevation $\eta(x, t)$ is clearly more accurate near the maximum in $b(x)$ on the finer grid.) Bouchut computed this problem using four modern numerical schemes, on 200 point grids as described in [4]. Like the A4WS method, three of those four methods (all but the VFRoe scheme) are free of spurious oscillations in the depth H near the stationary shock, and all of the methods are free from oscillations in H over the rapidly varying bathymetry. However, the three most accurate methods exhibit much larger oscillations in HU to varying degrees near the shock when compared to A4WS (see Table 2 or figures 6.6–6.10 in [4]).

Table 2 shows the l_∞ error for hu for the transcritical shock problem for the A4WS method and the three accurate methods tested in [4], indicating the degree to which the steady state is maintained at given grid resolution. The error for the other three methods is interpreted from figures in [4], and is therefore only roughly approximate. (The single grid cell containing the shock is omitted from the error calculation in all cases, since the value of HU in that cell is immaterial due to the intermediate depth.) The error using A4WS with 50 grid points is also shown for comparison.

6.3. Test of tsunami propagation and inundation

In this section we introduce a one-dimensional problem as a test for modeling tsunami propagation and inundation. The bathymetry is a simple idealization of an ocean basin and continental shelf, and the initial profile reflects the scales of a typical tsunami. We perform this test on a one-dimensional grid with non-uniform fixed grid spacing to enable inundation modeling on a much finer grid than deep ocean propagation. Although we typically use adaptive mesh refinement for real tsunami simulations (*e.g.* [29,15,14,16]), the one-dimensional fixed non-uniform grids were chosen to facilitate future comparisons.

Table 2
The l_∞ error for hu for the A4WS method is compared to that of three methods tested in [4], using 200 grid points

Method	l_∞ error for hu	$(l_\infty$ error for $hu)/h$	$(l_\infty$ error for $hu)/\Delta x$
A4WS	3.89×10^{-5}	1.18×10^{-4}	3.07×10^{-4}
Suliciu [4]	$\approx 1.1 \times 10^{-2}$	$\approx 3.3 \times 10^{-2}$	$\approx 8.8 \times 10^{-2}$
Kinetc [4]	$\approx 5.0 \times 10^{-3}$	$\approx 1.5 \times 10^{-2}$	$\approx 4.0 \times 10^{-2}$
Hydrostatic[4]	$\approx 7.5 \times 10^{-3}$	$\approx 2.7 \times 10^{-2}$	$\approx 6.0 \times 10^{-2}$
A4WS (50 points)	1.43×10^{-4}	4.32×10^{-4}	2.85×10^{-4}

The A4WS error using 50 points is also shown.

This problem is computed in units of kilometers, on $0 \leqslant x \leqslant 3200$. The bathymetry is given by

$$b(x) = \begin{cases} -4.120 + 3e^{-(\frac{x-2500}{50})^2} + 4e^{-(\frac{x-3000}{50})^2}, & \text{if } x < 3000, \\ -0.120 + 10^{-3}(x - 3000), & \text{if } 3000 \leqslant x \leqslant 3100, \\ -0.020 + 10^{-1}(x - 3100), & \text{if } 3100 \leqslant x \leqslant 3100.4, \\ 0.020 + 10^{-3}(x - 3100.4), & \text{if } 3100.4 \leqslant x. \end{cases} \tag{64}$$

As shown in Fig. 5, the function (64) gives an ocean basin 4.120 km deep that is punctuated by a mid-ocean ridge at $x = 2500$, and rapid continental rise that transitions to a gradual (0.1%) linearly sloping continental shelf at $x = 3000$. At $x = 3100$ a steeper (10%) linear beach interrupts the gradual continental shelf for 400 m, rising from -20 to $+20$ m. These dimensions roughly reflect real ocean bathymetry in magnitude and scale, though this bathymetry is obviously much smoother than real bathymetry and topography. We computed this problem using a grid with three different spacings. In the deep ocean region, $0 \leqslant x \leqslant 2900$, we used grid cells with $\Delta x = 1$ (km). Over the continental shelf, $2900 \leqslant x \leqslant 3100$, $\Delta x = 0.1$ (km), and for the beach, $3100 \leqslant x \leqslant 3100.4$, $\Delta x = 0.5 \times 10^{-3}$ (km). This allows the inundation to be accurately and efficiently resolved on 0.5 m grid cells. (We used a variable Δt, equal on all grid spacings, with a maximum Courant number of 0.99 for each time-step.)

The initial tsunami displacement is given by

$$\eta(x, 0) = \begin{cases} 10^{-4}(x - 1000)e^{-(\frac{x-1000}{100})^2}, & \text{if } 500 \leqslant x \leqslant 1500, \\ 0, & \text{otherwise}, \end{cases} \tag{65}$$

which gives the initial depth $h(x, 0) = \eta(x, 0) - b(x)$. The initial momentum is zero ($hu(x, 0) = 0$). The initial profile, shown in Fig. 6(a), gives a disturbance approximately 4 m in amplitude and about 500 km in extent, reminiscent of the initial profile of a fairly large teletsunami.

The numerical challenges of this problem are: (1), accurately resolving the small deviation from the steady state that is the tsunami propagating over thousands of kilometers, (2), robustly and accurately capturing near-shore propagation containing incident and reflected bores, and (3), resolving the wet–dry interface that represents the moving shoreline during inundation. Note that the ratio of tsunami amplitude to ocean depth is $\approx 10^{-3}$ (smaller than some of the relative errors in hu shown in Tables 1 and 2), and the grid spacing is roughly equivalent to the ocean depth. This implies that Riemann problems near the tsunami are very nearly steady-state data on a very coarse grid, and resolving the tsunami requires precisely preserving this steady-state data. Fig. 6 shows the propagating tsunami and near-shore inundation at several times. As can be seen in frame (b), near-linear propagation occurs over much of the domain, before nonlinear compression, steepening and reflection, seen in frame (c). The initial inundation of the beach, from $t \approx 14000$–16000 (s), occurs with two incident bores which are subsequently reflected seaward as seen in frames (d)–(f). The inundation is also shown in Fig. 7, which shows run-up as a function of time.

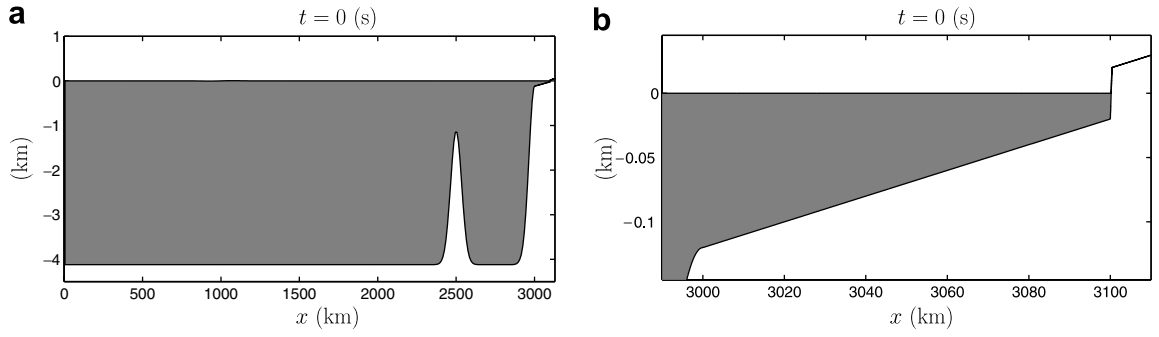

Fig. 5. Bathymetry for the idealized ocean basin and continental shelf. (a) Entire domain. (b) Close-up of the continental shelf and beach.

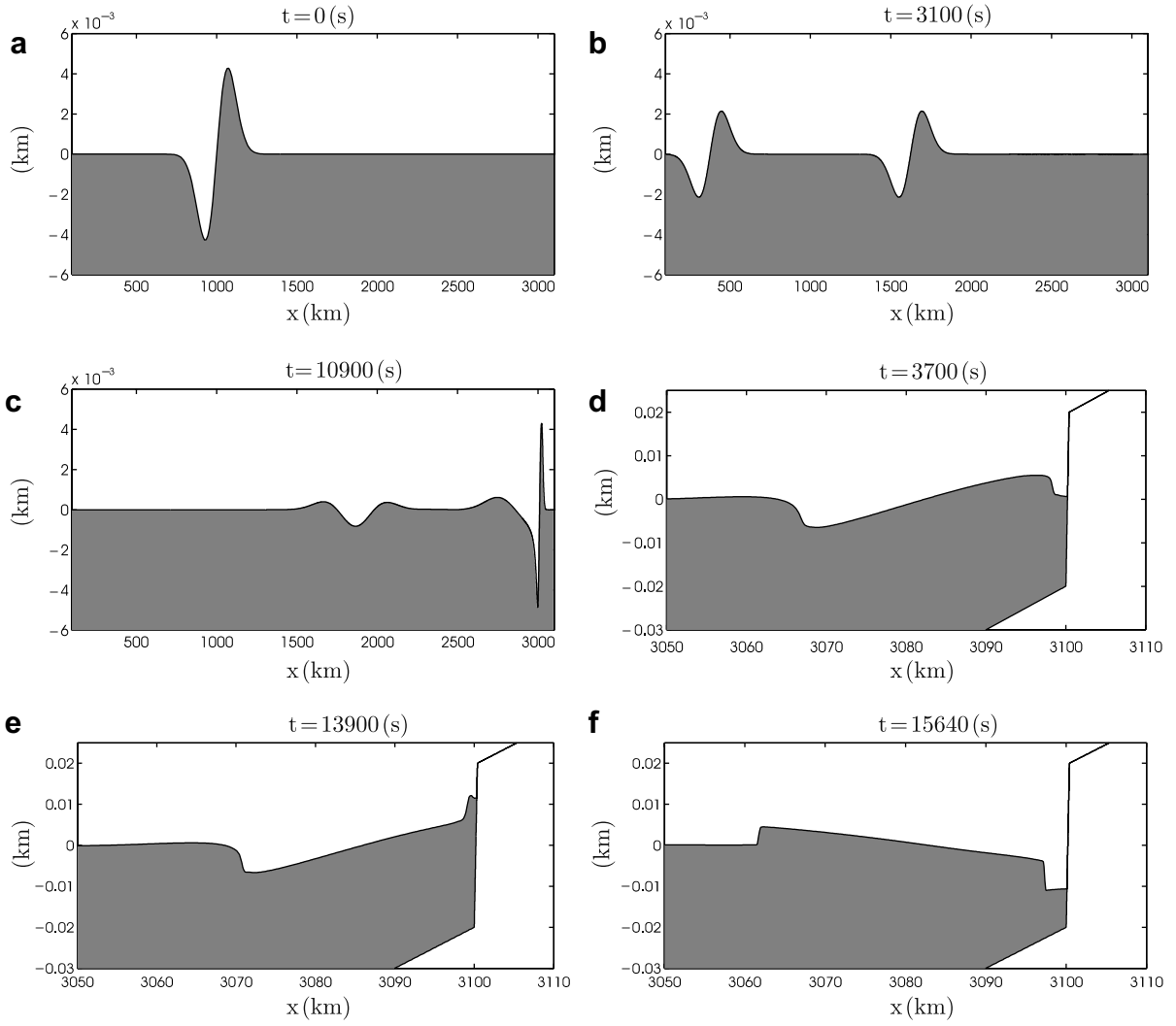

Fig. 6. Tsunami propagation. Figures show $\eta(x,t)$ at six different times. (a) The initial displacement. (b) The initial wave divides and propagates in each direction, leading to deep ocean amplitudes $\approx$2 m. (c) The wave is compressed and heightened as it approaches the shallow continental shelf, and reflected waves from the mid-ocean ridge can be seen propagating to the left. (d) Close-up showing the initial wave approaching the beach. (e) The beach near the time of maximum run-up from the first incident bore, which is reflected seaward. (f) A second bore approaches the beach as the first reflected bore on the left propagates seaward.

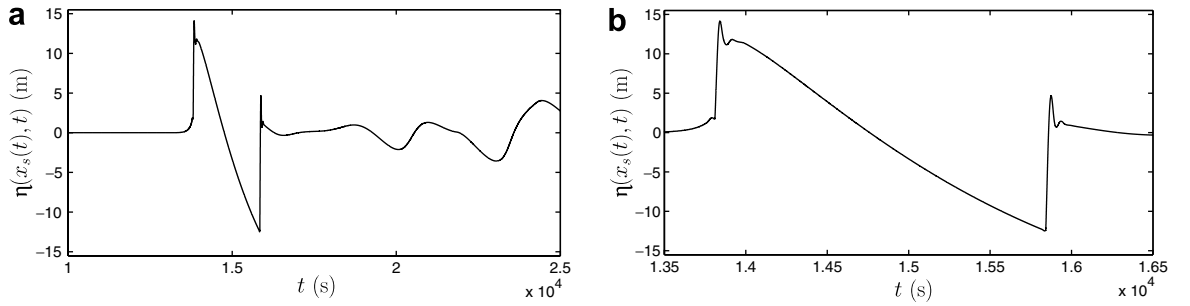

Fig. 7. Run-up at the shoreline as a function of time. (a) The height of the shoreline $\eta(x_s(t),t)$, where $x_s(t)$ denotes the horizontal location of the shoreline, is plotted as a function of time. Run-up of over 10 m occurs indicating a horizontal inundation of over 100 m. The effects of the incident bores can be seen at $t \approx 13700$ s and $t \approx 15800$ s. (b) Closer view of the maximum run-up and draw down period.

7. Conclusions

We have described an approximate Riemann solver for the shallow water equations that decomposes an augmented state variable—the depth, momentum, momentum flux, and bathymetry into four propagating discontinuities or waves. By using all four of these quantities in the decomposition, and by defining the eigenvectors used for decomposition appropriately, we are able to maintain several nice features in the approximate solution. First, large rarefactions are automatically divided into two discontinuities—providing a more accurate approximate solution for such problems and a natural entropy fix for transonic rarefactions. Second, shock-wave solutions are captured since the solver is equivalent to the Roe solver for such Riemann problems. Third, discretized smooth steady states over variable bathymetry, and the motionless ocean at rest steady state over any bathymetry, are exactly preserved since the Riemann decomposition in such a case contains only a stationary discontinuity, or steady state wave. Finally, the solver preserves depth non-negativity in the Riemann solution since it is equivalent to the HLLE solver (for mass) when source terms are absent, and by imposing suitable bounds on the stationary eigenvector in the presence of a source term. These properties make the solver appropriate for modeling the shallow water equations when steady states and dry cells exist, such as in the context of tsunami propagation and inundation modeling. These properties are accomplished when the solver is implemented with LeVeque's wave propagation algorithms [25].

Acknowledgements

The author would like to thank Randall LeVeque for his many valuable suggestions. This work was supported in part by NSF Grants CMS-0245206, DMS-0106511, and DOE Grant DE-FC02-01ER25474.

Appendix A

Proof of Theorem 1. In this appendix we prove Theorem 1. Consider a smooth steady state between two points, x_l and x_r, surrounding varying bathymetry. (We will use subscripts $()_l$ and $()_r$ on variables to denote evaluation at x_l or x_r respectively. Additionally, we will use Δ to denote differencing such quantities, $\Delta() = ()_r - ()_l$.) For all smooth steady states $(hu)_x \equiv 0$, and therefore

$$\Delta(hu) = 0. \tag{A.1}$$

Using this fact, we can relate the difference in the momentum flux,

$$\Delta\varphi = \varphi(q_r) - \varphi(q_l), \tag{A.2}$$

to the difference in the depth $\Delta h = (h_r - h_l)$. We write (A.2) explicitly, and rearrange, denoting $hu = hu_r = hu_l$,

$$\begin{aligned}\Delta\varphi &= \left(hu^2 + \frac{g}{2}h^2\right)_r - \left(hu^2 + \frac{g}{2}h^2\right)_l = \left(\frac{(hu)^2}{h_r} - \frac{(hu)^2}{h_l}\right) + \frac{g}{2}(h_r + h_l)(h_r - h_l)\\ &= \left(\frac{|(hu)_r(hu)_l|}{h_r} - \frac{|(hu)_l(hu)_r|}{h_l}\right) + \frac{g}{2}(h_r + h_l)(h_r - h_l)\\ &= (h_l|u_r u_l| - h_r|u_l u_r|) + \frac{g}{2}(h_r + h_l)(h_r - h_l) = \Delta h\left(-|u_r u_l| + \frac{g}{2}(h_r + h_l)\right),\end{aligned} \tag{A.3}$$

where $h \geqslant 0$ and $hu_r = hu_l$ together imply that $u_r u_l = |u_r u_l|$. We therefore have across the steady state

$$\Delta\varphi = -\widetilde{\lambda^+\lambda^-}(q_r, q_l)\Delta h. \tag{A.4}$$

We will later show that Δh must be non-zero (assuming that Δb is non-zero).

We can also relate Δh to Δb for smooth solutions. Note that for a steady state

$$\left(hu^2 + \frac{g}{2}h^2\right)_x = -ghb_x. \tag{A.5}$$

Together $(hu)_x = 0$ and (A.5) imply that

$$(-u^2 + gh)h_x = -ghb_x. \tag{A.6}$$

Note that (A.6) implies that a (smooth) sonic point cannot occur over varying bathymetry, and furthermore that h_x must be non-zero over varying bathymetry. Again, for steady states, (A.6) and $(hu)_x = 0$ imply that

$$\left(\frac{1}{2}\frac{(hu)^2}{h^2} + gh + gb\right)_x = 0, \tag{A.7}$$

which implies that

$$\left(\frac{1}{2}u^2 + gh + gb\right)_r = \left(\frac{1}{2}u^2 + gh + gb\right)_l. \tag{A.8}$$

Multiplying (A.8) by $\bar{h} = \frac{1}{2}(h_r + h_l)$ and rearranging gives,

$$\begin{aligned}
-g\bar{h}\Delta b - g\bar{h}\Delta h &= \left(\frac{h_r + h_l}{2}\right)\left(\frac{u_r^2 - u_l^2}{2}\right) = \left(\frac{1}{2}\right)^2\left(h_r u_r^2 + h_l u_r^2 - h_r u_l^2 - h_l u_l^2\right) \\
&= \left(\frac{1}{2}\right)^2\left((2h_r u_r^2 - h_r u_r^2) + h_l u_r^2 - h_r u_l^2 - \left(2h_l u_l^2 - h_l u_l^2\right)\right) \\
&= \left(\frac{1}{2}\right)^2\left((2h_l u_l u_r - h_r u_r^2) + h_l u_r^2 - h_r u_l^2 - (2h_r u_r u_l - h_l u_l^2)\right) \\
&= \left(\frac{1}{2}\right)^2\left((h_l u_l^2 + 2h_l u_l u_r + h_l u_r^2) - (h_r u_l^2 + 2h_r u_l u_r + h_r u_r^2)\right) \\
&= \left(\frac{1}{2}\right)^2\left(h_l(u_r + u_l)^2 - h_r(u_r + u_l)^2\right) = -\left(\frac{u_r + u_l}{2}\right)^2\Delta h,
\end{aligned} \tag{A.9}$$

where the fourth equality makes use of $h_l u_l = h_r u_r$. Eq. (A.9) implies the relationship

$$(-\bar{u}^2 + g\bar{h})\Delta h = -g\bar{h}\Delta b, \tag{A.10}$$

where $\bar{u}$ is the arithmetic average $\frac{1}{2}(u_l + u_r)$. Eq. (A.10) is a discrete representation, or Taylor series of (A.6), using special averages. It is equivalent to

$$\overline{\lambda^+\lambda^-}(q_l, q_r)\Delta h = g\bar{h}\Delta b. \tag{A.11}$$

Note that (A.1), (A.4) and (A.11) together imply that for a smooth steady state over varying bathymetry, where $\Delta b \neq 0$, the following difference is satisfied:

$$\Delta\begin{bmatrix} h \\ hu \\ \varphi \\ b \end{bmatrix} = \Delta b\begin{bmatrix} \frac{g\overline{H}(q(x_l,t),q(x_r,t))}{\overline{\lambda^+\lambda^-}(q(x_l,t),q(x_r,t))} \\ 0 \\ -g\widetilde{H}(q(x_l,t),q(x_r,t)) \\ 1 \end{bmatrix}. \tag{A.12}$$

Note that the derivation of (A.1), (A.4) and (A.11) did not require bathymetry with a net variation, only a smooth steady state. However, for the case where $\Delta b \neq 0$, the terms in the vector on the right hand side of (A.12) are always defined since $\overline{\lambda^+\lambda^-}(q_l, q_r)$ cannot be zero, which follows from (A.11). (Of course, if $\Delta b = 0$, the form of $w^0_{i-1/2}$ is irrelevant since no source term appears in such a Riemann problem.)

Appendix B. Brief summary of the determination of the Riemann structure

In this appendix we provide a brief summary of the procedure for determining the structure of the exact Riemann solution for the shallow water equations. (By "structure of the exact Riemann solution", we mean

whether each characteristic field has a shock or rarefaction.) We provide this for completeness and convenience to the reader—for the derivation of the formulas and further explanation, see [37] or [14]. The structure of the Riemann problem can be determined by evaluating a nonlinear function, using the initial Riemann data, H_i, H_{i-1}, U_i and U_{i-1}. (We ignore the case where $H_i = 0$ or $H_{i-1} = 0$, since then the Riemann structure is known to be a single rarefaction.) We first define

$$\phi(h; H_i) = \begin{cases} 2(\sqrt{gh} - \sqrt{gH_i}) & \text{if } h \leqslant H_i, \\ (h - H_i)\sqrt{\frac{g}{2}\left(\frac{1}{h} + \frac{1}{H_i}\right)} & \text{if } h > H_i \end{cases} \tag{B.1}$$

for $h > 0$. Now we define the function

$$\Phi_{i-1/2}(h) = \phi(h; H_i) + \phi(h; H_{i-1}) + U_i - U_{i-1} \tag{B.2}$$

for $h > 0$. Since $\Phi_{i-1/2}(h)$ is a monotonically increasing function of h (see [37]), the Riemann structure is determined by establishing one of the following three possibilities:

$$\text{Case 1}: \quad \Phi_{i-1/2}(H_{\min}) \leqslant \Phi_{i-1/2}(H_{\max}) \leqslant 0 \Longleftrightarrow \text{two shocks}, \tag{B.3}$$

$$\text{Case 2}: \quad \Phi_{i-1/2}(H_{\min}) < 0 < \Phi_{i-1/2}(H_{\max}) \Longleftrightarrow \text{shock and rarefaction}, \tag{B.4}$$

$$\text{Case 3}: \quad 0 \leqslant \Phi_{i-1/2}(H_{\min}) \leqslant \Phi_{i-1/2}(H_{\max}) \Longleftrightarrow \text{two rarefactions}, \tag{B.5}$$

where $H_{\max} = \max(H_i, H_{i-1})$ and $H_{\min} = \min(H_i, H_{i-1})$. In then event of CASE 2, $H_{i-1} < H_i$ implies a shock in the first family, and $H_{i-1} > H_i$ implies a shock in the second.

Additionally, the root of $\Phi_{i-1/2}(h)$ corresponds to the middle state depth:

$$\Phi(H^*_{i-1/2}) = 0. \tag{B.6}$$

In the event of CASE 3, the root can be exactly determined by solving for h in (B.2), giving

$$H^*_{i-1/2} = \frac{1}{16g}\left(2\max(0, \sqrt{gH_i} - \sqrt{gH_{i-1}} - U_i + U_{i-1})^2\right). \tag{B.7}$$

For Case 2, the root of the linear secant connecting $\Phi_{i-1/2}(H_{\min})$ to $\Phi_{i-1/2}(H_{\min})$ gives a good approximation to the true middle state depth $H^*_{i-1/2}$, and is always greater than the true middle state depth since $\Phi_{i-1/2}(h)$ is convex.

References

[1] M. Arora, P.L. Roe, On postshock oscillations due to shock capturing schemes in unsteady flows, J. Comput. Phys. 130 (1) (1997) 25–40.

[2] E. Audeusse, F. Bouchut, M.O. Bristeau, R. Klein, B. Perthame, A fast and stable well-balanced scheme with hydrostatic reconstruction for shallow water flows, SIAM J. Sci. Comput. 25 (6) (2004) 2050–2065.

[3] D.S. Bale, R.J. LeVeque, S. Mitran, J.A. Rossmanith, A wave propagation method for conservation laws and balance laws with spatially varying flux functions, SIAM J. Sci. Comput. 24 (2002) 955–978.

[4] F. Bouchut, Nonlinear Stability of Finite Volume Methods for Hyperbolic Conservation Laws and Well-Balanced Schemes for Sources, Birkhäuser Verlag, 2004.

[5] P. Brufau, P. García-Navarro, Unsteady free surface flow simulation over complex topography with a multidimensional upwind technique, J. Comput. Phys. 186 (2003) 503–526.

[6] P. Brufau, M.E. Vázquez-Céndon, P. García-Navarro, A numerical model for the flooding and drying of irregular domains, Int. J. Numer. Methods Fluids 39 (2003) 247–275.

[7] M. Castro, J.M. Gallardo, C. Parés, High order finite volume schemes based on reconstruction of states for solving hyperbolic systems with nonconservative products. Applications to shallow water systems, Math. Comput. 75 (255) (2006) 1103–1134.

[8] A.I. Delis, Th. Katsaounis, Relaxation schemes for the shallow water equations, Int. J. Numer. Methods Fluids 41 (2003) 695–719.

[9] B. Einfeldt, On Godunov-type methods for gas dynamics, SIAM J. Numer. Anal. 25 (1988) 294–318.

[10] B. Einfeldt, C.D. Munz, P.L. Roe, B. Sjogreen, On Godunov-type methods for near low densities, J. Comput. Phys. 92 (1991) 273–295.

[11] T. Gallouët, J.M. Hérard, N. Seguin, Some approximate Godunov schemes to compute shallow water equations with topography, Comput. Fluids 32 (2003) 479–513.

[12] P. García-Navarro, M.E. Vázquez-Céndon, On numerical treatment of the source terms in the shallow water equations, Comput. Fluids 29 (2000) 17–45.

[13] D.L. George, Numerical Approximation of the Nonlinear Shallow Water Equations: a Godunov-type Scheme, Master's Thesis, University of Washington, Seattle, WA, 2004.
[14] D.L. George, Finite Volume Methods and Adaptive Refinement for Tsunami Propagation and Inundation, Ph.D. Thesis, University of Washington, Seattle, WA, 2006.
[15] D.L. George, R.J. LeVeque, Finite volume methods and adaptive refinement for global tsunami propagation and local inundation, Sci. Tsunami Hazard. 24 (5) (2006) 319–328.
[16] D.L. George, R.J. LeVeque, High resolution methods and adaptive refinement for tsunami propagation and inundation, in: Hyperbolic Problems: Theory, Numerics, Applications, Proceedings of the 11th International Conference on Hyperbolic Problems, in press.
[17] S.K. Godunov, A difference method for numerical calculation of discontinuous solutions of the equations of hydrodynamics, Mat. Sb. 47 (1959) 271–306.
[18] N. Goutal, F. Maurel (Eds.), Proceedings of the Second Workshop on Dam-break Wave Simulation, Chatou, France, 1997, EDF/DER HE-43/97/016/B.
[19] J.M. Greenberg, A.Y. LeRoux, R. Barraille, A. Noussair, A well-balanced scheme for numerical processing of source terms in hyperbolic equations, SIAM J. Numer. Anal. 33 (1) (1996) 1–16.
[20] J.M. Greenberg, A.Y. LeRoux, R. Barraille, A. Noussair, Analysis and approximation of conservation laws with source terms, SIAM J. Numer. Anal. 34 (5) (1997) 1980–2007.
[21] A. Harten, P.D. Lax, B. van Leer, On upstream differencing and Godunov-type schemes for hyperbolic conservation laws, SIAM Rev. 25 (1983) 235–261.
[22] S. Jin, X.P. Xin, The relaxation schemes for systems of conservation laws in arbitrary space dimensions, Commun. Pure Appl. Math. 48 (1995) 235–276.
[23] S. Karni, S. Canić, Computations of slowly moving shocks, J. Comput. Phys. 136 (1997) 132–139.
[24] A. Kurganov, D. Levy, Central upwind schemes for the St. Venant system, Math. Modell. Numer. Anal. 36 (2002) 397–425.
[25] R.J. LeVeque, Wave propagation algorithms for multi-dimensional hyperbolic systems, J. Comput. Phys. 131 (1997) 327–335.
[26] R.J. LeVeque, Balancing source terms and flux gradients in high-resolution Godunov methods: the quasi-steady wave-propagation algorithm, J. Comput. Phys. 146 (1998) 346–365.
[27] R.J. LeVeque, Finite Volume Methods For Hyperbolic Problems. Texts in Applied Mathematics, Cambridge University Press, Cambridge, 2002.
[28] R.J. LeVeque, D.L. George, The Geoclaw software package. Freely available at: <http://www.geoclaw.org>.
[29] R.J. LeVeque, D.L. George, High-resolution finite volume methods for the shallow water equations with bathymetry and dry states, in: C. Synolakis P. L-F. Liu, H. Yeh, (Eds.), Advanced Numerical Models for Simulating Tsunami Waves and Runup, in press.
[30] R.J. LeVeque, M. Pelanti, A class of approximate Riemann solvers and their relation to relaxation schemes, J. Comput. Phys. 172 (2001) 572–591.
[31] J. Murillo, J. Burguete, P. Brufau, P. García-Navarro, Coupling between shallow water and solute flow equations: analysis and management of source terms in 2D, Int. J. Numer. Methods Fluids 49 (2005) 267–299.
[32] J. Murillo, P.J. García-Navarro, J. Burguete, P. Brufau, A conservative 2D model of inundation flow with solute transport over dry bed, Int. J. Numer. Methods Fluids 52 (2006) 1059–1092.
[33] J. Murillo, P.J. García-Navarro, J. Burguete, P. Brufau, The influence of source terms on stability, accuracy and conservation in two-dimensional shallow flow simulation using triangular finite volumes, Int. J. Numer. Methods Fluids 54 (2007) 543–590.
[34] P.L. Roe, Approximate Riemann solvers, parameter vectors, and difference schemes, J. Comput. Phys. 43 (1981) 357–372.
[35] P.K. Sweby, High resolution schemes using flux limiters for hyperbolic conservation laws, SIAM J. Numer. Anal. 21 (1984) 995–1011.
[36] E.F. Toro, Riemann Solvers and Numerical Methods for Fluid Dynamics, Springer-Verlag, Berlin, 1997.
[37] E.F. Toro, Shock Capturing Methods for Free Surface Shallow Flows, Wiley and Sons, United Kingdom, 2001.